LASER-INDUCED DAMAGE IN OPTICAL MATERIALS

Concetto R. Giuliano, et al

Hughes Research Laboratories

Prepared for:

Advanced Research Projects Agency
Air Force Cambridge Research Laboratories

February 1974

LASER-INDUCED DAMAGE IN OPTICAL MATERIALS

By

CONCETTO R. GIULIANO
ROBERT W. HELLWARTH

HUGHES RESEARCH LABORATORIES
3011 MALIBU CANYON ROAD
MALIBU, CALIFORNIA 90265

CONTRACT F19628-72-C-0348
PROJECT 2042

FINAL REPORT
15 JUNE 1972 - 15 DECEMBER 1973

FEBRUARY 1974

CONTRACT MONITOR : HAROLD POSEN
SOLID STATE SCIENCES LABORATORY

Sponsored by
DEFENSE ADVANCED RESEARCH PROJECTS AGENCY
ARPA ORDER 2042

Monitored by
AIR FORCE CAMBRIDGE RESEARCH LABORATORIES
AIR FORCE SYSTEMS COMMAND
UNITED STATES AIR FORCE
BEDFORD, MASSACHUSETTS 01730

ARPA Order No.	2042
Program Code No.	3D10
Contract No.	F19628-72-C-0348
Contractor	Hughes Research Laboratories
Effective Date of Contract	15 June 1972
Contract Expiration Date	15 December 1973
Principal Investigator	Dr. Concetto R. Giuliano (213)456-6411, Ext. 437
AFCRL Project Scientist	Dr. Harold Posen (615)861-3532

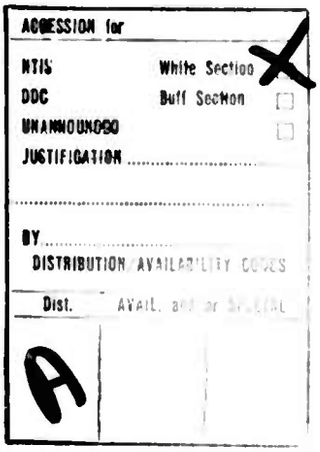

Qualified requestors may obtain additional copies from the Defense Documentation Center. All others should apply to the National Technical Information Service.

PREFACE

We wish to acknowledge the essential contributions of individuals who have contributed to the results presented in this document. Discussions with V. Evtuhov, B. Soffer, and V. Wang were often helpful in providing critical evaluation of various aspects of this work and providing ideas for choosing the direction taken at a number of junctures. Technical assistance by T. Horne and G. Rickel is also greatfully acknowledged. H. Garvin has contributed in a number of ways including the ion beam polishing of sapphire and suggesting and providing the sputtered sapphire coatings on proustite. J. Potosky has performed ion polishing and plasma sputtering of lithium niobate and has carried out and evaluated a number of detailed damage measurements on this material. P. Fleming, R. Hart, and E. Wolf provided scanning electron micrographs of surface features and electron microprobe data on proustite.

Unclassified
Security Classification

AD-777146

DOCUMENT CONTROL DATA - R&D

(Security classification of title, body of abstract and indexing annotation must be entered when the overall report is classified)

1. ORIGINATING ACTIVITY *(Corporate author)*
Hughes Research Laboratories
3011 Malibu Canyon Road
Malibu, California 90265

2a. REPORT SECURITY CLASSIFICATION
Unclassified

2b. GROUP

3. REPORT TITLE
LASER-INDUCED DAMAGE IN OPTICAL MATERIALS

4. DESCRIPTIVE NOTES *(Type of report and inclusive dates)*
Scientific. Final. 15 June 1972 through 15 December 1973

Approved 3 Mar74

5. AUTHOR(S) *(First name, middle initial, last name)*
Concetto R. Giuliano
Robert W. Hellwarth

6. REPORT DATE
February 1974

7a. TOTAL NO. OF PAGES
~~104~~ 106

7b. NO. OF REFS
43

8a. CONTRACT OR GRANT NO. ARPA Order No. 2042
F19628-72-C-0348

b. PROJECT, TASK, WORK UNIT NOS.
2042 n/a n/a

c. DOD ELEMENT
62701E

d. DOD SUBELEMENT n/a

9a. ORIGINATOR'S REPORT NUMBER(S)

9b. OTHER REPORT NO(S) *(Any other numbers that may be assigned this report)*
AFCRL-TR-74-0104

10. DISTRIBUTION STATEMENT
Approved for public release; distribution unlimited.

11. SUPPLEMENTARY NOTES
This research was supported by the Defense Advanced Research Projects Agency

12. SPONSORING MILITARY ACTIVITY
Air Force Cambridge Research Laboratories (LQ)
L.G. Hanscom Field
Bedford, Massachusetts 01730

13. ABSTRACT

This report contains the results of damage experiments performed on 0.694 and 1.06 μm using well-controlled Q-switched ruby and Nd:YAG lasers. Materials studied at 1.06 μm are proustite (Ag_3AsS_3) and lithium niobate ($LiNbO_3$). Surface damage thresholds were measured for proustite for different conditions of pulse repetition rate and pulse duration. Attempts to improve damage resistance via different optical finishing techniques showed little or no improvement for proustite, but a low reflectivity sputtered sapphire film appears to yield a significant increase (~40%) in damage threshold. Electron microprobe studies were performed showing evidence for chemical decomposition around catastrophic proustite damage sites. Attempts to use ion beam polishing, a process that improved sapphire damage resistance markedly, showed little or no improvement for $LiNbO_3$ samples. However, sputtering of LiNbO in an $Ar\text{-}O_2$ rf-excited plasma showed up to a 40% increase in damage threshold over the untreated surface in a preliminary experiment. Damage in both proustite and lithium niobate appears to be limited by inclusions and not an intrinsic property of the material studied. Experiments at 0.694 μm were concentrated on a comparison of the temporal profiles of transmitted pulses with back-reflected, Brewster reflected, and small-angle backscattered pulses. It was found that a marked increase in backscattered light occurs at the time of damage as indicated by a cutoff in the transmitted pulse. This method of detection is the most sensitive indication of the occurrence of damage we have found; a distinct change in backscattered light temporal profile is seen, even when the transmitted pulse shows no detectable change. Attempts to use these measurements to find evidence for precatastrophic damage show a definite effect, but one that is so subtle that it does not represent a practical indication of a damage precursor. A discussion of the theories of optical avalanche breakdown is presented in which doubts are raised as to whether "intrinsic" breakdown has ever been observed. Arguments are presented that support the likelihood that ionic impurities play a crucial role in optical breakdown.

DD FORM 1 NOV 65 1473

Unclassified
Security Classification

14. KEY WORDS	LINK A		LINK B		LINK C	
	ROLE	WT	ROLE	WT	ROLE	WT
Laser damage						
Surface damage						
Proustite						
Lithium niobate						
Sapphire						
0.694 and 1.06 μm						
Surface conditioning						
Ion polishing						
Single mode laser						
Reflected pulse temporal studies						
Scattered pulse temporal studies						
Temporal and Spatial irregularities						
Avalanche breakdown						
Damage morphology						
RF plasma conditioning						

TABLE OF CONTENTS

LIST OF ILLUSTRATIONS

I. INTRODUCTION AND SUMMARY

In this report we present the results of research on fundamentals of laser induced damage in optical materials. The problem of optical damage has been given considerable attention by a number of investigators since the earliest reports[1] and continues to be the limiting factor that determines the successful operation of high power lasers and laser systems. Because of the use of poorly controlled lasers employed in early damage investigations, there has been a great deal of disagreement between the damage thresholds reported by different workers. This has often been compounded by a lack of reproducibility in material quality and detailed characterization as well. Since assignment of an energy or power density requires a knowledge of the laser beam spatial properties, an accurate determination of laser spot size is required. The means by which different investigators determine laser spot sizes vary considerably and differences in flux densities obtained from these spot size determinations can disagree widely. Hence, a few years ago, it became evident that more meaningful results would be forthcoming if damage studies were performed with lasers having well characterized spatial and temporal properties.

The first such investigations were initiated at Hughes Research Laboratories in an ARPA-sponsored program followed by other investigations at different laboratories. Bulk and surface damage in a variety of materials have been investigated under a number of different conditions and at several wavelengths. Rather than offer an extensive bibliography of published work in laser damage, we refer the reader to the proceedings of recent laser damage conferences.[2-5] The recent work performed at HRL is described in two recent contract final reports[6,7] and in a number of journal publications.[8-17]

This report contains results of continuing experiments on laser-induced damage in optical materials. The emphasis has been on surface damage and the wavelengths of interest have been 0.694 μm and 1.06 μm. Proustite (Ag_3AsS_3) and lithium niobate have been studied

principally at 1.06 μm. Work on these materials is described in Sections II-B and II-C. Primary interest in these materials has been to explore the possibility of improving damage resistance by different surface conditioning techniques. Because the damage observed in these materials appears to be inclusion limited, we were not able to evaluate conclusively the efficacy of the surface conditioning techniques employed, but certain ones appear to be promising. Namely, sapphire-coated proustite shows up to a 40% improvement over the uncoated surface, and lithium niobate that has been sputtered in an rf-excited argon-oxygen plasma shows a similar improvement over the conventionally polished material.

The studies carried out at 0.694 μm using a single mode ruby laser (Section II-D) have been directed toward a more detailed understanding of the dynamics of surface damage formation and accompanying phenomena. The possibility for detecting precursory effects that would signal the onset of damage prior to the catastrophic event was explored in a variety of ways. Although no well-defined reproducible precursory phenomena were found, we did discover an extremely sensitive means of detecting the onset of the most subtle kind of surface damage; light scattered back at small angles from the irradiated surface shows a large increase from the background level at the onset of damage, an effect that is easily detected even when there is no detectable change in the level of light transmitted through the sample.

Sections II-E and II-F give detailed descriptions of the lasers used on the damage program and the techniques employed to characterize their spatial beam properties.

Section III discusses the theories of optical breakdown that have gained prominence over the years and raises important objections as to whether "intrinsic" dielectric breakdown via electron avalanche has actually been observed. Arguments are presented that support the likelihood that ionic impurities, now known to exist in the best crystals studied to date, play a crucial role in optical breakdown.

II. EXPERIMENTAL STUDIES OF LASER-INDUCED SURFACE DAMAGE

A. Experimental Procedure for Damage Threshold Measurements

In all the damage threshold measurements carried out on this program, a specific procedure was followed to obtain the desired data. The sample was prepared in a prescribed way (see below) and inspected with the aid of a microscope for cleanliness and quality of surface finish. Then it was mounted so that it could be accurately positioned relative to the focusing lens with respect to both lens-to-sample distance and to transverse position of the beam relative to any point on the surface. (A He-Ne alignment laser was used as an aid for locating the desired point on the surface in the sapphire damage experiments. It was not used with proustite because it was discovered earlier[7] that proustite is damaged by microwatt levels of illumination at 6328 Å.)

The desired location on the surface of the sample was exposed initially to a level of Q-switched laser illumination chosen to be appreciably below damage threshold. Then the sample was examined using a low-power (20 to 30x) microscope that can be moved in and out without disturbing the sample. If no damage was observed after several shots at a given level, the power was increased (by 5 to 15%) and the sample irradiated again, and so on until damage occurred. The power at which damage was seen to occur according to this procedure was taken to be damage threshold. We outline the experimental procedure in detail, because later it will be an important factor in the light of some observations made on proustite.

B. Laser-Induced Surface Damage in Proustite (Ag_3AsS_3)

1. Introduction and Summary

Because of its nonlinear optical properties, proustite (Ag_3AsS_3) is an especially attractive material for parametric oscillators[18-20] and infrared up-converters.[21-23] However, its propensity for being rather easily damaged has generated some doubts as to its

value for high power applications. During this program we have continued investigations of proustite damage begun on another program[7] in order to obtain some clues as to the nature of its laser damage mechanisms and to better evaluate it as a candidate for nonlinear optical applications.

For the sake of completeness we will include briefly results obtained earlier (Sections II-B-3-a and b) as well as the work which we performed on this program. We begin with a description of the interesting morphology of different kinds of surface damage for proustite. Then the results of many damage experiments are described for different conditions of pulse repetition rate and pulse duration. Effects of surface finish are discussed as well as other phenomena observed in which the surface damage resistance is seen to change with time and past history of laser exposure. Some promising results for improving the damage resistance of proustite are presented for sputtered sapphire (Al_2O_3) films which seem to protect the surface from general deterioration as well as improve its damage threshold. The results of electron microprobe measurements are presented which show conclusive evidence for chemical changes accompanying the more catastrophic types of damage. This technique was also used to probe for the presence of absorbing impurities which may have accumulated on the surface from fabrication polishing or surface cleaning techniques. (None were detected.)

The general conclusion of the proustite study is that the ultimate damage resistance has probably not been reached in presently available materials. Most of the evidence obtained in this study supports the conclusion that damage in the proustite studied in this program is caused by absorption by inclusions or other small defects in the material.

2. Damage Morphology in Proustite

Three distinctly different types of damage are seen on proustite entrance surfaces. The occurrence of a particular type depends on the character of the irradiation (i.e., whether pulsed or

continuous) and also to some extent on the quality of the surface finish. The three types are described in the following paragraphs.

a. Molten Craters – These have been seen to occur only during cw illumination at relatively high cw powers or when a previously created pulse damage site is illuminated with a relatively low cw power. The formation of these craters is accompanied by a plume of yellow smoke (presumably sulfur), which sometimes settles on the undamaged surface in the vicinity of the crater, depending on the direction of air currents in the laboratory. The craters have slightly raised rims and relatively flat shiny bottoms that appear black in color and are apparently the result of molten puddles of decomposed material. Crater depth is typically 25 μm. This type of damage is the most catastrophic of the three types observed. Examples of this type of damage are seen in Figs. 1 and 2 where we present optical and scanning electron micrographs.

By being especially vigilant while irradiating the sample with continuous illumination at 1.06 μm, it is possible to cut off the light incident on the sample before the catastrophic crater formation takes place. An example of the damage formed at inception is shown in the scanning electron micrographs in Fig. 2(a), 2(b), and 2(c) where we see evidence of some local melting in a region about 20 μm across.

b. Micromelting – This type of damage occurs with either single-pulsed or repetitively pulsed illumination. It is characterized by a series of somewhat randomly spaced tiny molten regions. The number and density of these regions depends on both the local surface finish and the incident power. When the power is appreciably above threshold, the molten regions merge to form a large variegated damage spot. At lower powers, there is tendency for these small globular sites to cluster along lines of surface scratches. When observed through the low-power microscope in the laboratory damage threshold setup, they appear to have a metallic luster, and the region in which they are clustered has a darker color than the surrounding undamaged surface. Figure 3 shows optical micrographs of proustite

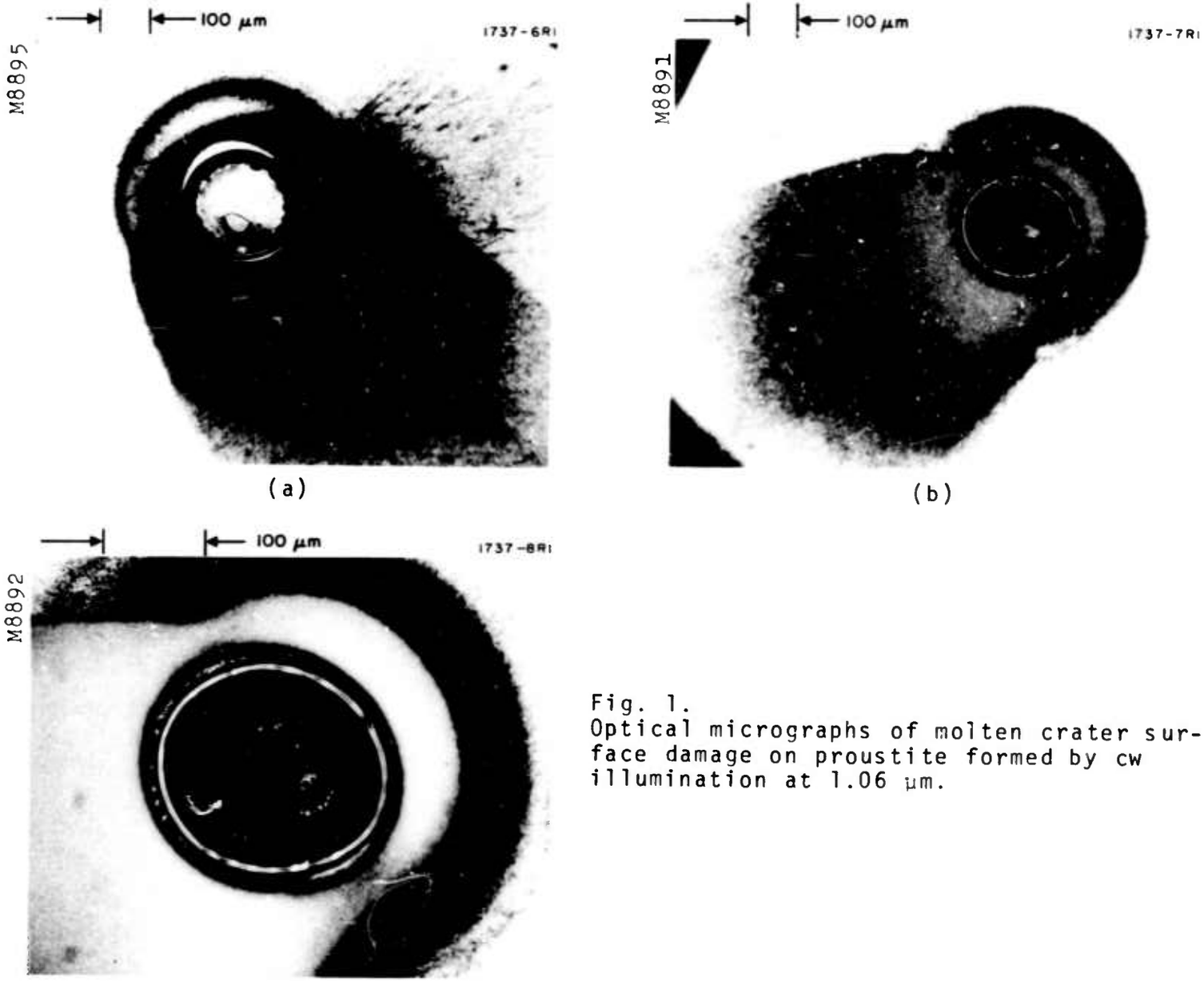

Fig. 1.
Optical micrographs of molten crater surface damage on proustite formed by cw illumination at 1.06 μm.

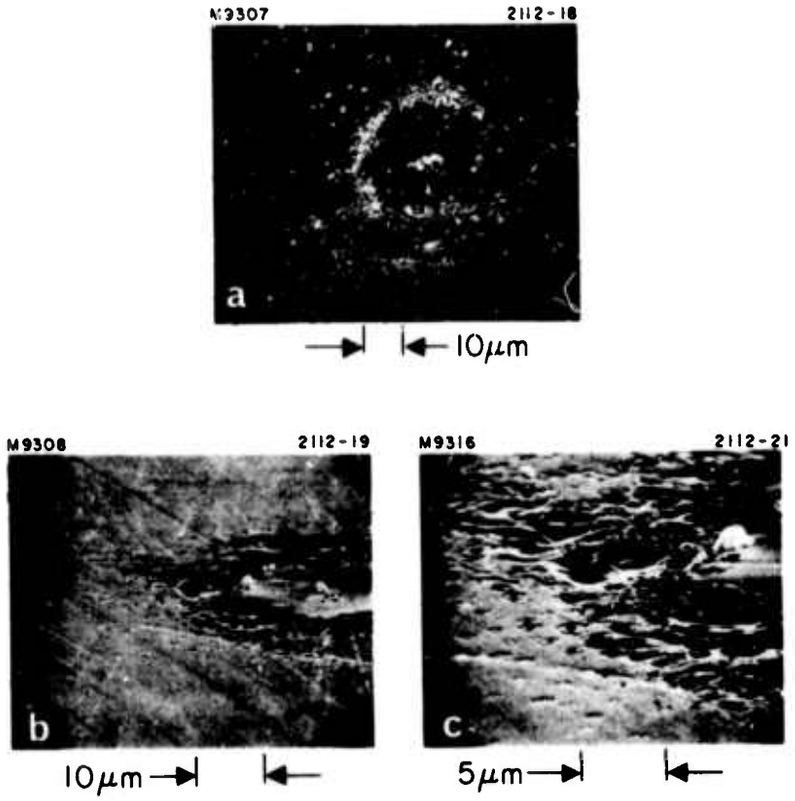

Fig. 2.
Scanning electron micrographs of molten crater damage on proustite formed by cw illumination at 1.06 μm. (a) A site formed close to threshold viewed at normal incidence. (b) and (c) Same site as (a) viewed at 70° from normal.

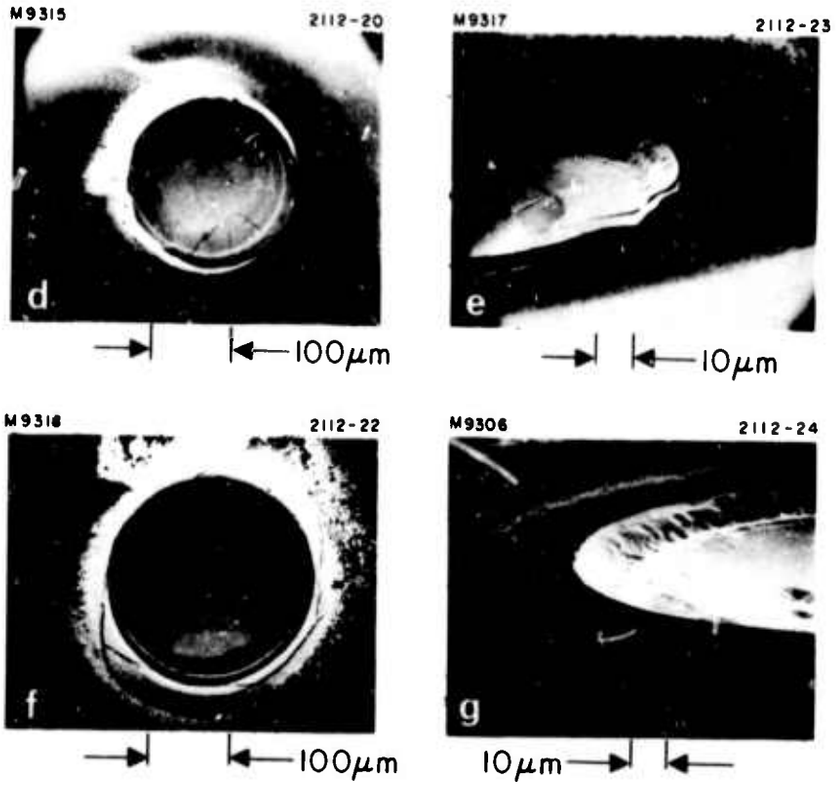

Fig. 2. (Continued).
(d) Normal view. (e) Same as (d) viewed at 70°.
(f) Normal view. (g) Same as (f) viewed at 70°.

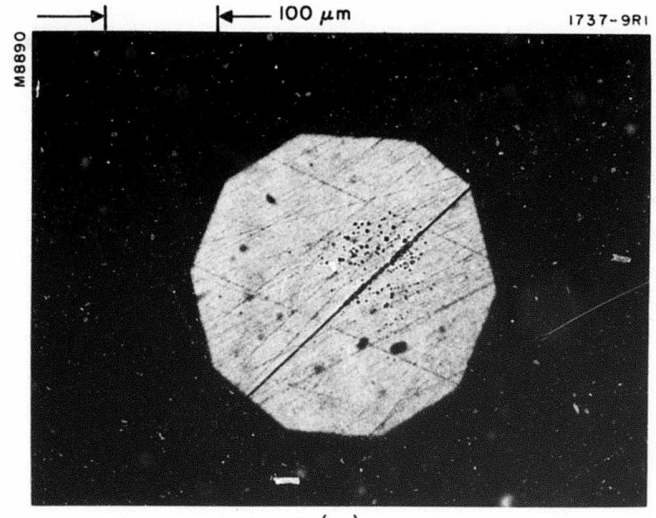

(a)

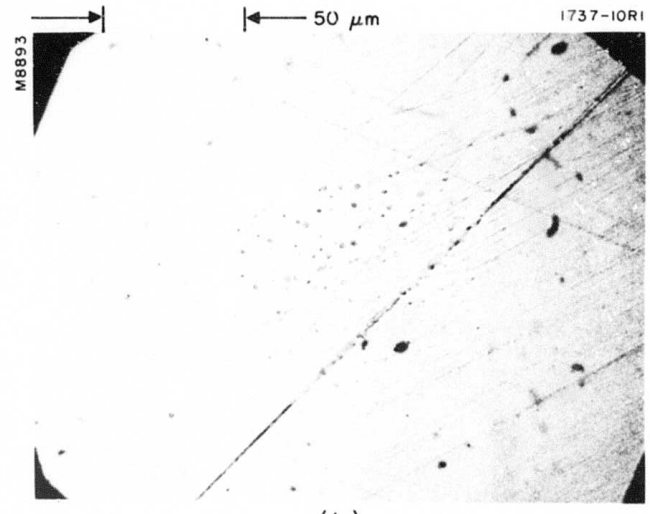

(b)

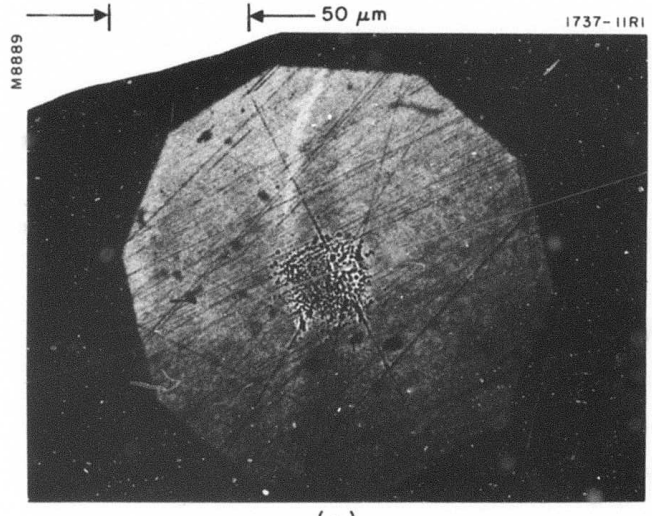

(c)

Fig. 3.
Optical micrographs of proustite surface damage generated by pulsed irradiation at 1.06 μm close to threshold.

damage formed close to threshold. Figure 4 shows scanning electron micrographs of proustite damage for both single and multiple pulses.

c. Ghost Sites – This type of damage occurs with continuous illumination at 1.06 μm and was a source of much confusion when first observed. Under low magnification in the laboratory setup, it is similar in appearance to the damage described in the preceding paragraph; that is, it appears as a speckled area with a metallic luster. This kind of damage is easily visible with the unaided eye as a small scattering region on the surface. Depending on the incident laser power and exposure time, however, the damage fades within 30 sec to 30 min after the laser is turned off and sometimes disappears completely. This type of damage happens at very low cw power, and as the power is increased, it takes longer to fade away until finally a power level is reached at which some of the damage appears to be permanent. Ghosting has been seen also at high repetition rate illumination, but only if the surface finish has the cloudy appearance referred to in the beginning of this section.

3. Results of Proustite Damage Experiments

a. Damage in Proustite for Continuous Illumination at 1.06 μm – As mentioned earlier, two kinds of damage occur with cw illumination: the molten craters and the speckled ghost sites. The first type occurs at relatively high cw powers and requires long exposure times (sometimes several minutes) before suddenly occurring. The conditions under which it occurs (power and exposure time) vary so drastically that we were unable to obtain meaningful quantitative data. A threshold for the latter type of damage also was difficult to define, but it is possible to quote some limiting conditions under which it occurs. The power density for which this speckling persists after five minutes was taken as one limit. This value is approximately 2.3 kW/cm^2. The power density at which no speckling was observable at all for several minutes of exposure is about 300 W/cm^2. Between these two values, the speckled ghost sites appear to varying degrees; after the laser is turned off, they fade and gradually disappear.

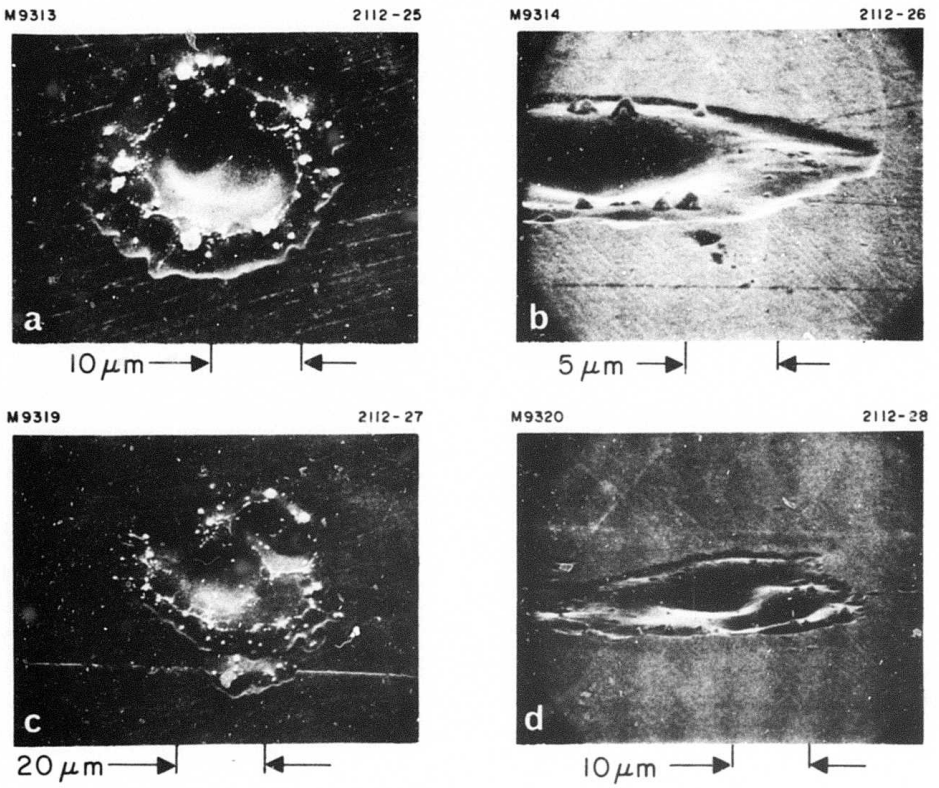

Fig. 4. Scanning electron micrographs of proustite surface damage generated by pulsed irradiation at 10.6 μm. The picture occurs in pairs showing a particular site viewed at normal incidence and at 70^{o} from normal. (a) through (d) were formed by single shot; (e) and (f) were formed by 10 shots; (g) and (h) were formed by 500 pps for 1 sec.

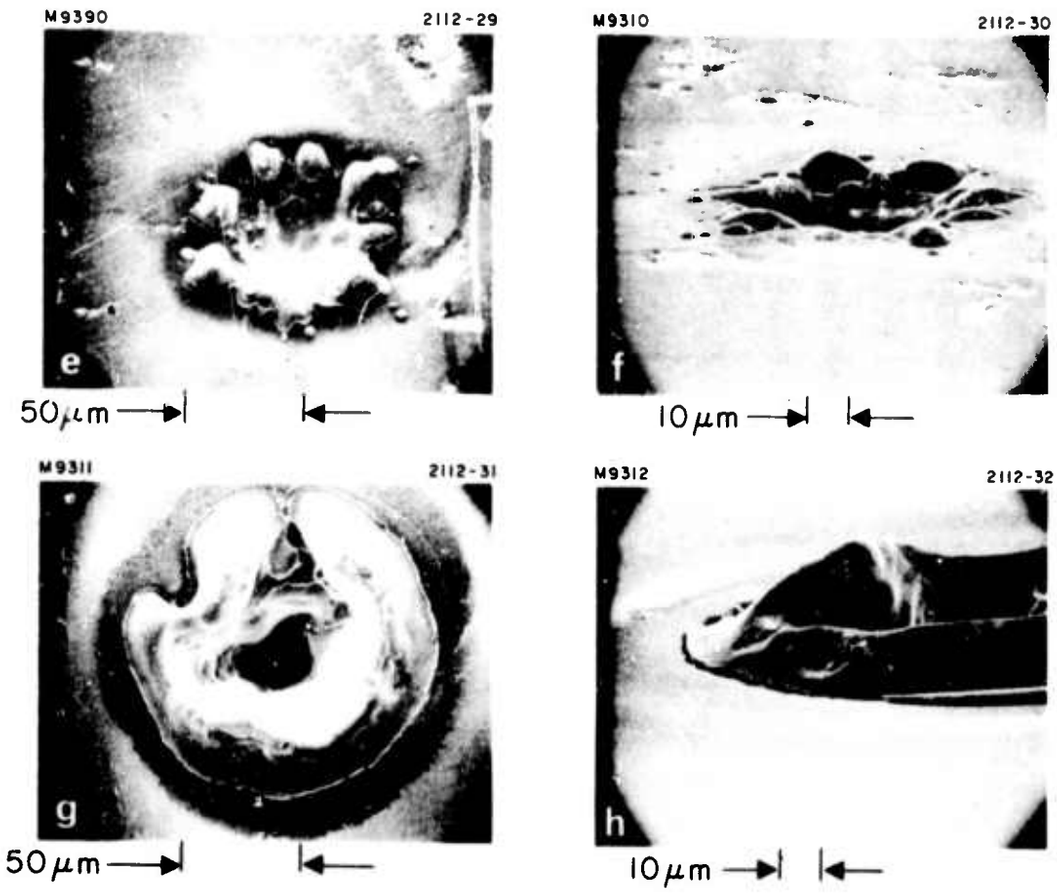

Fig. 4. Continued.

b. Damage Threshold in Proustite as a Function of Pulse Repetition Rate – A series of threshold measurements were carried out on proustite at different pulse repetition rates. All the measurements were taken on the same sample. The results of these measurements are presented in Table I. The damage threshold intensities listed are those levels for which damage was observed according to the procedure described earlier.

TABLE I

Damage Thresholds for Proustite as a Function of Pulse Repetition Rate

Pulse Repetition Rate	Relative Damage Threshold	Range	No. Thresholds Measured
Single shot	1.0	0.83 to 1.2	11
60 pps	1.02	0.87 to 1.2	1[illegible]
300 pps	0.94	0.84 to 1.1	16
500 pps	0.96	0.83 to 1.2	10

It should be pointed out here that most of the sites where damage was observed at a particular power level were subjected to a large number of shots at predamage powers, which were a few percent below the level at which damage was finally seen to occur. A typical example is a damage site which at 60 pps was subjected to over 4000 shots whose powers ranged in steps from 79 to 93% of the power at which damage finally occurred. We cite another example at 500 pps in which the site of interest was subjected to 30,000 nondamaging shots, whose powers ranged from 55 to 90% of the power at which damaged occurred. Hence, we interpret the range of threshold data obtained for proustite as reflecting a variation in surface damage resistance from point to point.

c. Optical Damage in Proustite at 1.06 μm for Pulses of Different Duration – One of the main interests for this study has been to measure the damage threshold for proustite at 1.06 μm for pulses of different duration in an attempt to obtain some insight into the nature of the damage mechanism. This was done on the same sample (sample A) using two different Nd:YAG lasers having pulse durations (FWHM) of about 20 nsec and 260 to 300 nsec. The results are presented in Table II along with data for other samples for comparison.

TABLE II

Entrance Surface Damage Thresholds in Proustite for Different Pulse Durations

Sample	λ, μm	Damage Threshold[a] Power Density MW/cm^2		Damage Threshold[a] Energy Density, J/cm^2	τ, Pulse Duration (FWHM), nsec	Beam Radius,[b] μm
		Av Value	Range[c]			
A	1.06	11.1	6.9-16.0	2.88	260-300	37.3
A	1.06	40.8	31-55	0.715	17.5	86.0
B	1.06	42.1	38-51	0.737	17.5	86.0
C[d]	1.06	1.61	1.4-1.9	0.40	300	74.0
(Ref. 24)	1.06	~29	-	0.50	17.5	650
D	0.694	60	54-69	1.08	20	56.0

[a] These values are given as total power (or energy) divided by the beam area defined as $\pi\alpha^2$, where α is the 1/e radius for the electric field. The on-axis intensities (energy densities) are twice as large as the values quoted in the table.

[b] Defined at the 1/e points for the electric field.

[c] These are the maximum and minimum values observed for a series of 25 to 30 measurements on a given sample.

[d] This is the sample for which data are given in Table 2.

The values for sample A in Table II show that the energy density for damage increases for longer pulses qualitatively suggesting a thermal mechanism. The ratio of damage threshold energy densities for sample A is proportional to $\tau^{1/2}$ which is indicative of either absorption in a thin surface layer[25] or absorption of short pulses by inclusions[26] or other types of absorbing centers. The surface damage morphology close to threshold as illustrated in Figs. 2 and 3 suggest that the latter mechanism is more likely.

The above conclusion is based on data taken at only two pulse durations and should be further investigated by obtaining points for pulse durations between 20 and 300 nsec. Recent unpublished results by other workers[27] indicate that the single shot damage threshold for proustite occurs at a constant energy density for pulses from 20 to 80 nsec, a result that would suggest that the half-power dependence is not operative in this time regime. This apparent disagreement can only be resolved by further detailed experiments over these pulse duration regimes.

The threshold data for sample C in Table II are substantially lower than those of the same pulse duration for sample A. Because past experience with different proustite samples has indicated a wide variation in properties both optical and otherwise from one sample to another, it is not surprising to see such a difference. In fact, it is more surprising to note the reasonably close agreement of threshold values obtained at 17.5 nsec pulse duration between our results and those of Hanna, et al.,[24] who used a much larger spot size than was used in our experiments. This fact, coupled with the observed damage morphology, further supports the mechanism of local absorption in regions that are small compared with the beam size.

d. Surface Finish of Proustite and Related Effects — Attempts to improve the surface finish of proustite by ion polishing on an earlier program[7] resulted in serious degradation of the material at the surface, presumably from a chemical decomposition. This occurred even at the lowest ion energies available. No further attempts at ion polishing on proustite were undertaken in this program.

We did, however, explore a few different abrasive polishing techniques for proustite with respect to polishing compound and lapping surface; a variety of results were obtained, mostly negative. For example, Syton, a Monsanto product which is an alkaline suspension of SiO_2 in water, was tried as a polishing compound. This material has been found to be an excellent polishing compound for a variety of materials from metals to refractory oxides and glasses, but on proustite the result was a blackening and severe etching of the surface presumably via a chemical reaction with the hydroxide ions.

Procedures that did result in improvement in surface quality were the use of 0.05 μm fumed silica in water using a medium pitch lap, as well as 0.05 μm γ-alumina in water on a pitch lap. The main difference between these polishing methods and the one used earlier is that a paraffin lap was used in the early polishing methods. Although some qualitative improvement was achieved in surface finish (e.g., lower density of scratches), there was not an appreciable increase in damage threshold.

Table III shows results obtained for different polishing conditions on the same sample.

Several features should be noted in discussing the results presented in Table III. First, the reason for the difference between the results obtained for the two spot sizes is not completely clear. The data were taken at different times, and the surface condition of the sample was not necessarily the same although it was prepared in the same manner. It is possible that the average value of damage threshold might be higher for a smaller spot size because the chance of encountering a low threshold region (assuming a certain distribution of absorbing inclusions) on each shot is less in general for a small spot than for a larger one. But one would expect that even though the average value might be higher, the range of values should overlap somewhat, especially on the low side (i.e., one should occasionally encounter low threshold regions with the small spot size as well). Of course, the number of thresholds measured is not large enough in these cases to preclude the possibility that this spot size effect is a reflection of the distribution of inclusions and/or surface defects.

TABLE III

Damage Threshold for Proustite Sample With Different Polishing Conditions (17.5 nsec pulse)

Polishing Conditions	Damage[a] Threshold, J/cm^2 (average value)	Range	Number of Thresholds Measured	Beam radius,[b] μm
γ-Al_2O_3 on paraffin	0.715	0.54 to 1.0	17	86
γ-Al_2O_3 on paraffin	1.12	1.00 to 1.28	11	49
Fumed silica on pitch	1.32	1.10 to 1.73	14	49
Fumed silica on pitch (fresh polish)	1.46	0.89 to 2.85	13	49

[a] These values are given as the total energy divided by the beam area defined as $\pi\alpha^2$ where α is the 1/e radius for the electric field. The energy densities on-axis are twice as large as the values quoted in the table.

[b] Defined at the 1/e points for the electric field (the $1/e^2$ points for the intensity) for a gaussian beam.

T976

Of more significance, however, is the last entry labeled "fresh polish." In most instances, as discovered earlier, the threshold measurements on proustite are carried out on samples that have been recently polished, usually on the same day. This practice was undertaken because it was found that the surface was seen to accumulate a cloudy appearance within a few hours of polishing when viewed with appropriate illumination under magnification. Typically, the damage thresholds would begin to drift downward as the cloudiness would develop; after one or two days of standing in air the threshold would level off to a value sometimes as much as a factor of two lower than those obtained in the first few hours of measurement.

This type of behavior was most striking in the series of experiments that resulted in the last entry in Table III (fresh polish). This phenomenon is illustrated in Fig. 5 which shows the threshold results as obtained sequentially for a series of spots on the sample surface each separated by 0.5 mm. The gradual dropoff referred to above can be seen in the figure.

The threshold value reported in Table III is an average of all the thresholds measured. However, it can be seen (Fig. 5) that the first few points measured result in lifting the average considerably. The total sequence of measurements illustrated in Fig. 5 represent about 100 shots of the laser and required most of a full day to carry out. This kind of behavior illustrates the difficulty one faces in obtaining meaningful damage threshold data for proustite.

e. Pretoughening of Proustite Surfaces Using Low-Power Illumination – The study of surface damage in proustite has been further complicated by a phenomenon observed recently in this program. The following behavior was noted while performing a series of damage experiments on a freshly prepared sample (Sample A, Table II) using the low-power Nd:YAG laser. The procedure outlined at the beginning of this section was used in obtaining data in which the desired region is irradiated with pulses of gradually increasing power until damage is observed. For several spots on the surface that were irradiated with a large number of low-power shots (15 to 20), we were unable to obtain damage with repeated pulses at the maximum power available from the laser. When the sample was moved slightly, so that the beam was allowed to strike a spot only about 50 μm away from the previously nondamagable location, damage invariably occurred on the first shot. Subsequent to observing this behavior, we carried out a different series of experiments where we held the output of the laser constant for a series of shots, each time hitting a different spot on the surface and examining for damage between shots. This was done over a range of incident power levels with about 20 shots taken at each level.

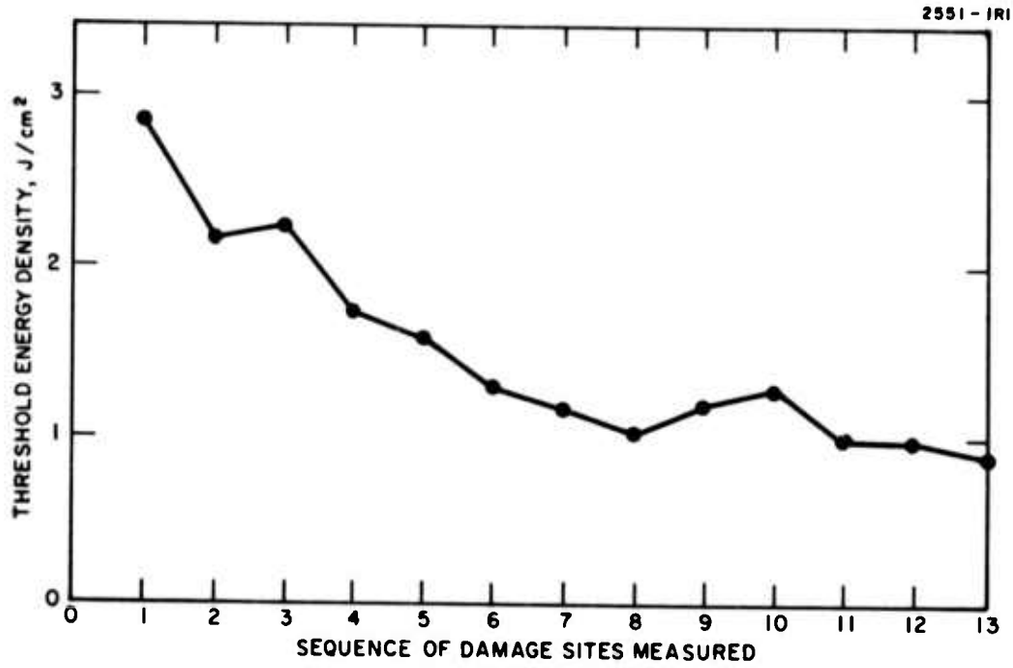

Fig. 5. Values of damage thresholds obtained in sequence on a freshly polished proustite surface.

In this series, damage was found to occur, on the average, at lower levels (30% lower) than for cases where the sample was preirradiated at low nondamaging powers.

This behavior was further complicated by the general gradual surface degradation always observed with proustite with exposure to the laboratory environment. Hence, after a few hours the preconditioning phenomenon seemed to disappear, or at least diminish appreciably to the point that the occurrence of damage at a given level seemed to be independent of whether the spot of interest had been pre-irradiated at lower levels.

We point out this behavior as an additional illustration of the complexity of damage behavior in proustite.

f. Surface Damage on Al_2O_3-Coated Proustite – Recently the idea arose that it might be advantageous to provide a protective coating for proustite that would result in better damage properties. The combined facts that sapphire (Al_2O_3) has a high damage threshold and a refractive index (1.76) that is close to the geometric mean between that of proustite (~3) and air made it a good potential candidate as a low-reflectivity, damage resistant coating for proustite.

A wafer of proustite about 15 mm diameter and 2 mm thick was coated in three different regions with sputtered Al_2O_3 coatings of different thicknesses: 1450 Å, 1700 Å, and 1970 Å which correspond to 0.24 λ, 0.28 λ, and 0.33 λ at 1.06 μm. A fourth region of the sample remained uncoated.

Damage threshold measurements were made on all four regions of the sample using the high-power Nd:YAG laser (pulse duration 17.5 nsec) focused on the entrance surface. The results of these measurements are presented in Table IV.

The damage threshold energy and power densities listed in the second and third columns of Table IV are the measured values incident

TABLE IV

Damage Thresholds for Al_2O_3-Coated Proustite

Region	Al_2O_3 Coating Thickness, Å	Damage Threshold[a] Energy Density, J/cm^2	Damage Threshold[a] Power Density, MW/cm^2	Measured Transmission, T	Intensity Reflection Coefficient at Entrance Surface, R	Corrected Threshold[a] Energy Density, J/cm^2
A	Uncoated	0.737 ± 6.5%[b]	42.1	0.324 ± 0.010[b]	0.204	0.587
B	1450	0.858 ± 8.9%	49.0	0.398 ± 0.018	0.0238	0.838
C	1700	0.729 ± 8.3%	41.5	0.413 ± 0.023	(-0.0151) ~0	0.729
D	1970	0.615 ± 10.6%	40.2	0.402 ± 0.013	0.0134	0.607

[a]These values are given as total power (or energy) divided by the beam area defined as $\pi\sigma^2$, where σ is the 1/e radius for the electric field. The on-axis intensities (energy densities) are twice as large as the values quoted in the table.

[b]The values listed are the average deviations taken from 25 to 30 measurements for each region.

upon the sample surface. However, because a fraction of the light is reflected from the sample, the actual energy available at the surface for creating damage should be multiplied by the quantity 1-R, where R is the intensity reflection coefficient. Therefore, a more valid comparison of the entrance surface damage thresholds for the coated regions compared with the uncoated region accounts for the difference in entrance surface reflectivities.

The reflectivities of the coated surfaces were not measured directly, but they can be obtained by a comparison of the measured transmissions as listed in Table IV. The energy transmission T of a slab of absorbing material having reflection coefficients at the entrance and exit surfaces of R_1 and R_2, respectively, is given by

$$T = \frac{(1 - R_1)(1 - R_2)e^{-\alpha d}}{1 - R_1 R_2 e^{-2\alpha d}} \qquad (1)$$

where d is the sample thickness and α is the absorption coefficient.

Using the above equation and the computed value for the reflectivity of the uncoated surface of R = 0.204 (from a value of the refractive index taken to be 2.65) it is possible to obtain the absorption loss and the reflectivities of the coated regions of the sample. The small negative reflectivity listed for region C is not real, of course, but a result of the experimental error in measurement of the transmissions and the assumption that the absorption and reflectivity are uniform throughout the sample.

The corrected threshold energy densities listed in Table IV are obtained by multiplying the appropriate measured value by $(1 - R_1)$. Here we see that all three coated regions have thresholds higher than the uncoated region, although the values for regions A and D lie within experimental error of each other.

In all cases, the damage of Al_2O_3-coated proustite occurs at the interface between the coating and the surface. Examples of this damage are given in Fig. 6. Figure 6(a) through (d) show examples of damage formed when the sample was irradiated at a level fairly close to threshold, whereas Figs. 6(e) and (f) are examples of damage found 2 to 3 times threshold. Figure 6(a) shows damage in the vicinity of a scratch on the proustite surface where the alumina film became separated from the surface prior to the damage formation. In all cases illustrated, the damage appears as small molten globules similar to that seen on the uncoated surface accompanied in most instances by film separation.

The moderate increase in threshold observed in some instances indicates that sapphire appears promising as a protective coating for proustite but it is evident that the quality of the proustite itself must be improved with regard to both freedom from impurities and inclusions and quality of surface finish. The nature of the observed damage

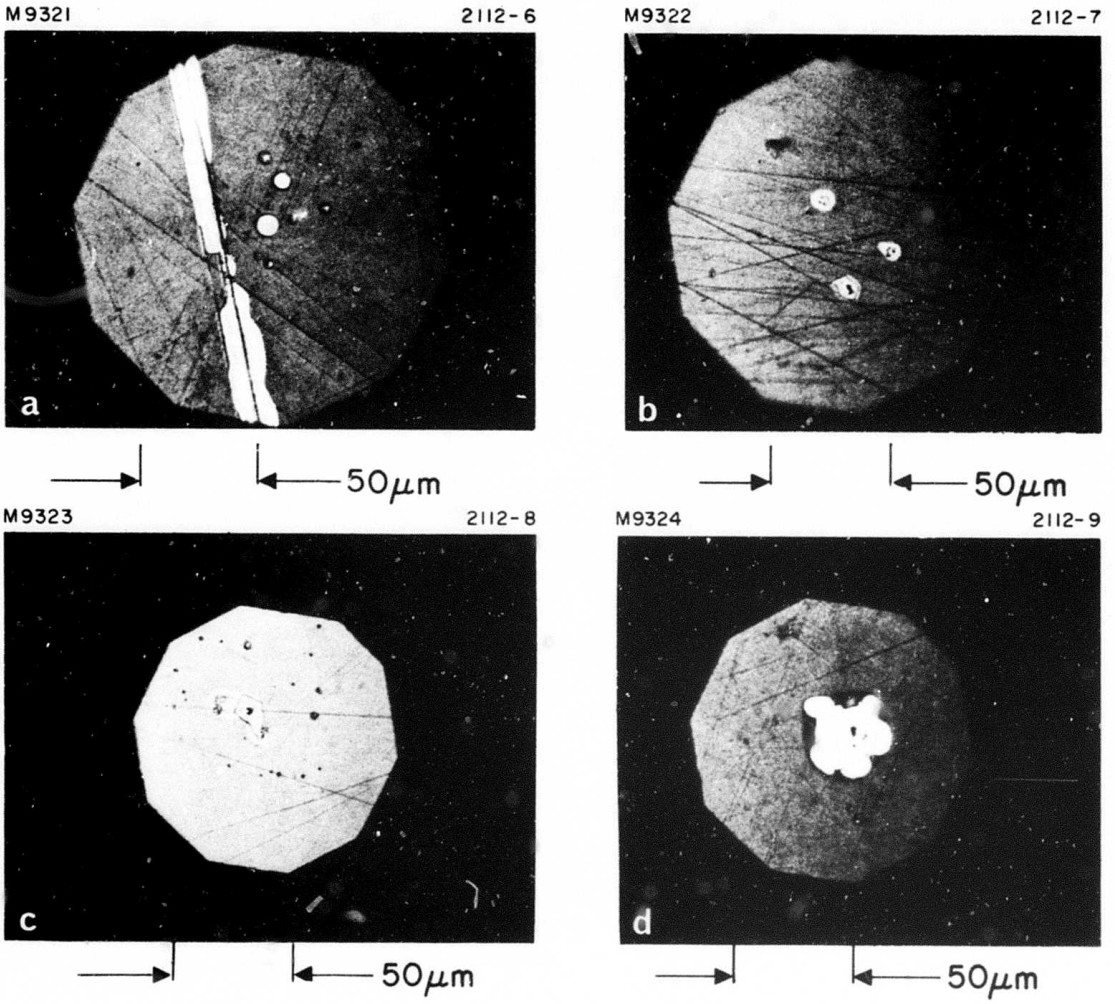

Fig. 6. Optical micrographs of damage on sapphire-coated proustite surface.

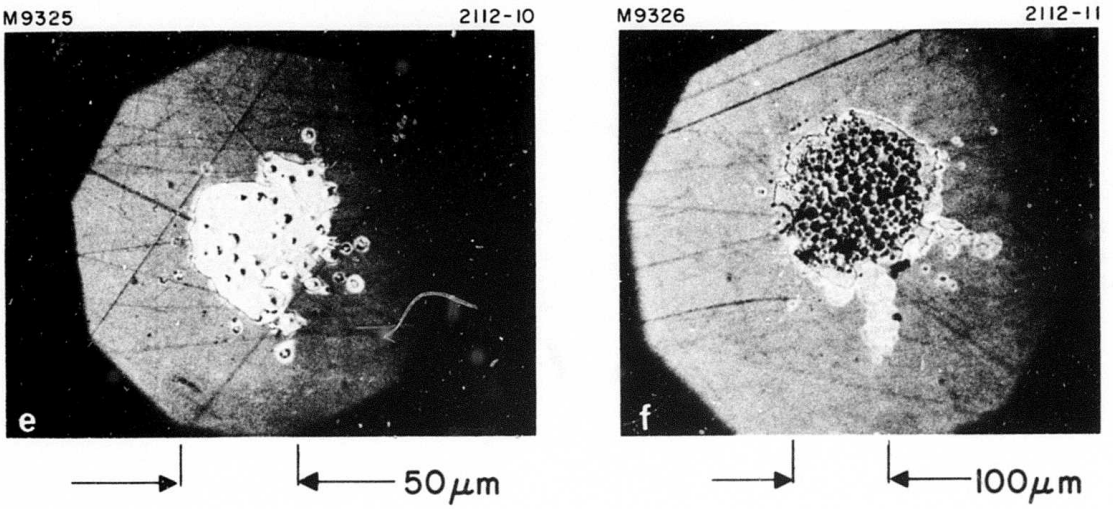

Fig. 6. Continued.

morphology strongly suggests that the damage threshold values obtained so far are not a measure of the intrinsic damage resistance of proustite, but indicate a limitation governed by impurities and/or inclusions as well as surface fabrication.

g. Proustite Damage on a Sample From a Different Source – In addition to the series of experiments just described, we had the opportunity to measure damage threshold on a proustite sample obtained from a different source than previous samples. Earlier proustite crystals were grown either at HRL or obtained from the Royal Radar Establishment (RRE). Samples from these sources had about the same damage threshold (within an average of ~50%) for similar conditions of pulse duration and focusing. Recently, we obtained a slice from a proustite boule grown by the British Drug House (BDH), formerly a supplier of raw material for proustite crystal growth.

The sample was polished by the technique described (fumed silica, pitch lap), and a series of surface damage threshold measurements was carried out.

As a comparison to the entries for the sample in Table III (an RRE sample), the BDH sample was damaged under the same focusing conditions as the latter entries (49 μm spot radius). The damage threshold energy density was 1.33 J/cm^2, an average of 27 different sites with values ranging from 1.0 to 1.7 J/cm^2.

One feature that distinguished the BDH sample from previously studied proustite samples is the morphology for surface damage formed near threshold. As illustrated in Semiannual Technical Report No. 1, the pulsed damage near threshold is usually characterized by a number of tiny molten areas clustered around surface scratches. Besides, the damage formed near threshold is rarely accompanied by the occurrence of a spark; surface sparks are usually seen on proustite if the incident energy is appreciably above threshold. For the BDH sample, however, the damage in all but 2 of the 27 cases observed consisted of a single surface pit and was accompanied by a spark.

The reason for this is not completely clear, but we believe it is an indication of a more uniform surface quality on this sample. The damage thresholds measured are not appreciably different from those measured under similar conditions for the RRE sample, but the fact that the morphology consisted of a single damage crater rather than a cluster of molten globules indicates that if the damage is limited by inclusions or other absorbing sites in the BDH sample they are more uniformly distributed than they are in the RRE samples studied.

h. Chemical Changes Accompanying Damage in Proustite – During this program we have explored the damage sites in proustite with respect to the possibility of chemical changes. As mentioned in the last report, the catastrophic surface damage caused by cw illumination is accompanied by a tiny plume of yellow smoke (presumably sulfur) emanating from the damage site.

This suggestion of chemical decomposition during laser damage led us to confirm it by other means and to determine whether similar decomposition might accompany other types of proustite surface damage (e.g., pulsed) as well.

To explore the surface composition we used an electron excited x-ray microprobe apparatus. This phenomenon employs a focused electron beam on the surface that locally excites atoms found in the beam. These excited atoms emit characteristic x rays that are measured in an x-ray spectrometer. The apparatus used has a scanning electron beam capability as well, and the different regions being probed can be displayed as on an electron microscope.

Results of a microprobe analysis are shown in Fig. 7. Here we see an electron micrograph of a damage site caused by cw illumination. Accompanying the micrograph is a series of dot patterns taken over the same region of the surface as seen in the micrograph. The brightness of the dot pattern in a given region is a measure of the amount of the element in question found in that region.

From these pictures we see (not surprisingly) that there is a definite chemical change accompanying this type of proustite damage.

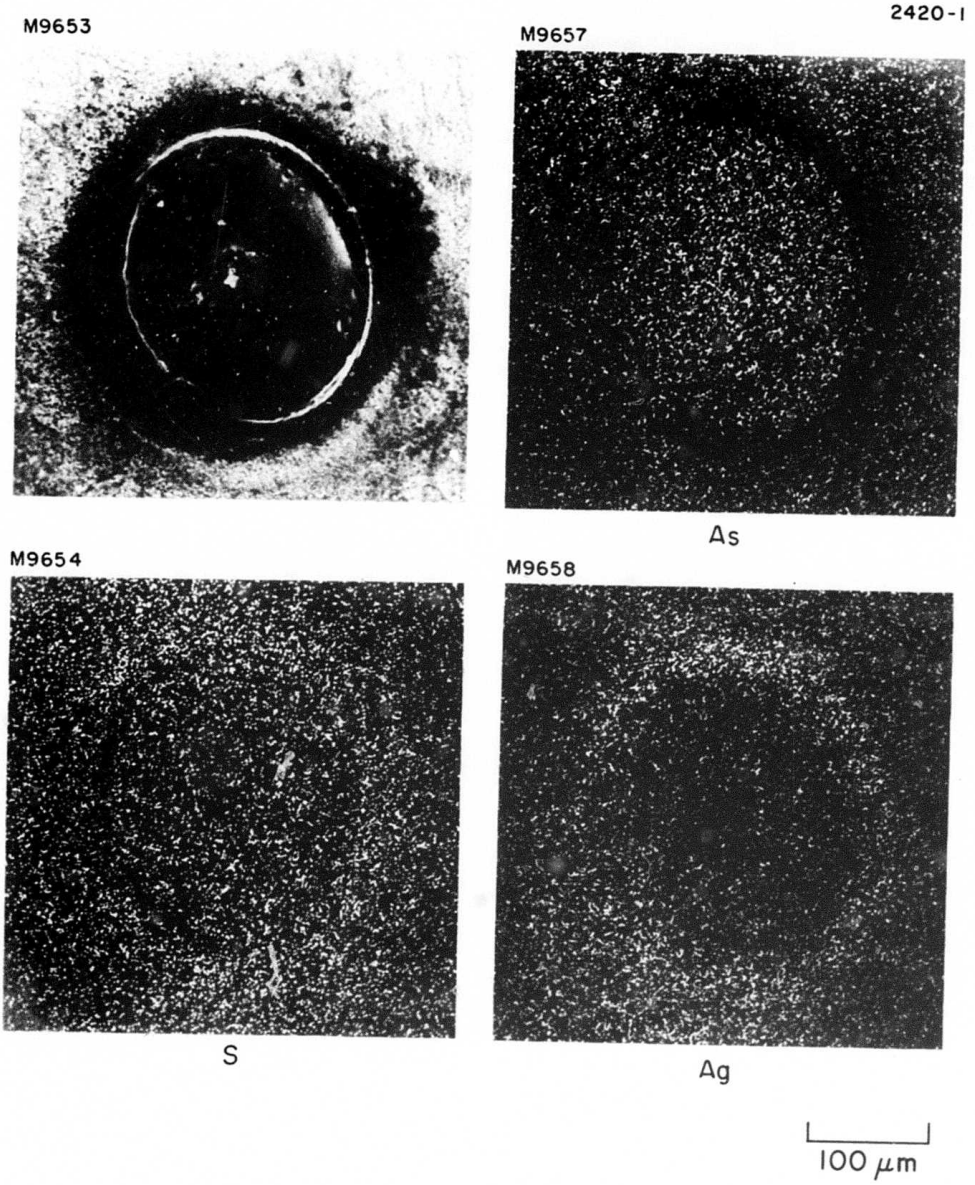

Fig. 7. Electron probe x-ray micrographs of a molten crater on proustite showing relative concentrations of Ag, As, and S.

There is, for example, a buildup of arsenic at the crater rim and a deficiency at the center. On the other hand, the center of the crater is rich in silver relative to the rim. The sulfur distribution is asymmetric as suggested by the yellow plume as indicated above.

Other types of proustite surface damage as illustrated in the last report were explored using the technique described above and no evidence for stoichiometric changes were seen in these experiments. Thus we conclude on the basis of this brief investigation that proustite damage is accompanied by chemical decomposition only for catastrophic effects caused by continuous illumination and not for pulsed illumination.

An added fact in connection with obtaining the above data is that proustite is damaged by the scanning electron beam used to excite the x-ray microprobe unless the beam current is kept at a relatively low value. An example of this type of e-beam damage is shown in Fig. 8. After this damage was observed all subsequent scans were preceded and followed by the taking of scanning electron micrographs (a very low current requirement). In this way the region of interest could be examined after the microprobe analysis was carried out to ensure that a nondamaging beam current was employed.

i. Search for Impurities in Proustite – We have also used the x-ray microprobe technique for exploring for the presence of surface contaminants. As reported earlier, the near threshold damage morphology for proustite surfaces shows small molten globules clustered around surface scratches. It is possible that these scratches or grooves could collect impurities that would be difficult to remove by conventional cleaning procedures or that they might contain particles of polishing compound.

Even though the polishing abrasives used (SiO_2, Al_2O_3) do not absorb 1.06 μm light, there is the possibility that the presence of abrasive particles on the surface could give rise to some increase in local absorption in the vicinity of surface scratches.

The electron beam x-ray microprobe apparatus was used to explore for the presence of impurities on the surface. For a given

2551-14

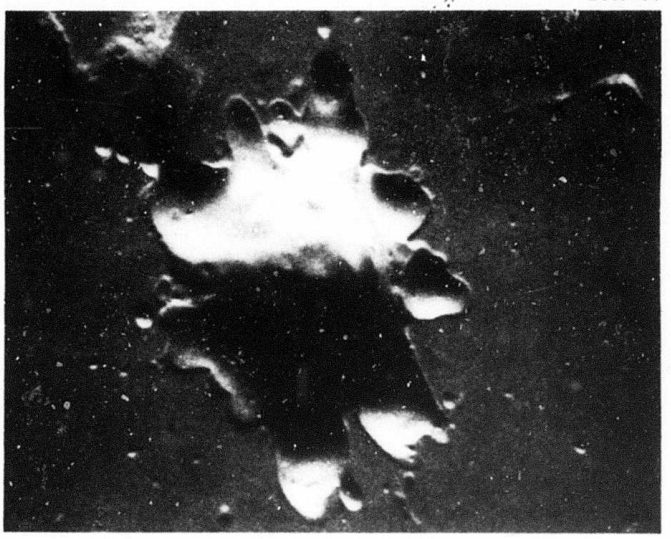

LASER DAMAGE CRATER

2551-15

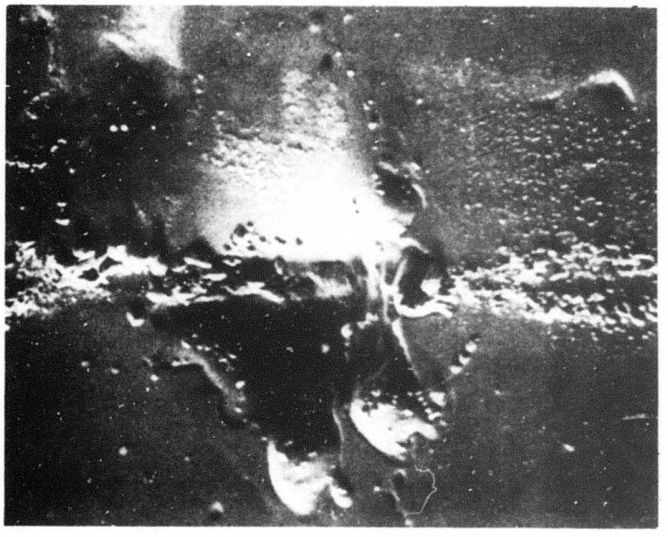

DAMAGE CRATER AFTER ELECTRON SCAN

10 μm

Fig. 8. Scanning electron micrographs of laser damage site on proustite before and after electron microprobe scan showing damage to proustite surface due to high current electron beam.

sample, many areas of the surface were scanned. Typically, the electron beam would illuminate a region of the surface 250 μm square and the x-ray spectrometer would scan over all the elements, the detector output being fed into a chart recorder. We have found from these measurements that except for a weak chlorine peak, there is no indication, within the sensitivity of this measurement (about 1 part in 10^3) of the presence of either aluminum or silicon.

Thus we conclude that there is no appreciable concentration of foreign impurities in the region of surface irregularities and that little or no abrasive particles are present in surface scratches or grooves.

C. Surface Damage in Lithium Niobate ($LiNbO_3$)

1. Ion Polishing Experiments

During the earlier phases of the program a number of experiments were performed on surface damage in $LiNbO_3$. The main thrust of this work was to explore the possibility of improving the surface damage threshold by ion polishing. The status of this work at present is inconclusive. A brief summary of the results obtained so far is that little or no improvement in damage threshold has been obtained yet on ion polishing. However, this result must be qualified by the observation that the damage seen so far in all the $LiNbO_3$ samples appears to be limited by inclusions. The quality of surface finish obtained by ion beam polishing is also strongly affected by the presence of surface inclusions.

Previous experience at HRL with ion sputtering of $LiNbO_3$ has led to a distinct sequence of steps used in the ion polishing experiments carried out during this period. Briefly described, the initial removal of material is carried out at a relatively high ion energy followed by exposures of lower ion energy toward the end of the treatment. The latter stages act as a kind of annealing treatment; if they are not performed, the sample is left with a substantial surface charge layer believed to be caused by a deficiency of oxygen at the surface.

All ion polishing treatments carried out were performed in the following sequence:

3 kV for 80 min at 140 $\mu A/cm^2$

1 kV for 60 min at 140 $\mu A/cm^2$

0.5 kV for 30 min at 70 $\mu A/cm^2$

An argon ion beam was used. The beam strikes the surface at an angle of 70° from normal and the sample is rotated during exposure to the beam.

All the samples studied were ion polished on one end only. Damage thresholds were carried out on the ion polished end and compared with measurements performed on the abrasively polished end. All damage measurements were taken with the 3.3 cm lens using the output from the Nd:YAG laser at 1.06 μm. The pulse duration was 17.5 nsec and the spot size at the sample surface was 49 μm (1/e radius for electric field). Damage threshold power densities are presented in Table V.

We see from the data in Table V that the ion polished surfaces have typically lower damage thresholds than the abrasive polished surfaces. In continuing work in this area we decided to employ lighter ion beam exposures than used earlier. Four different lithium niobate samples were abrasively polished on both ends to give uniformly finished surfaces of excellent quality. One end of each sample was then polished by ion bombardment for times varying from 30 to 180 min at beam energies from 0.5 to 1.0 keV and Ar^+ current densities from 50 to 200 $\mu A/cm^2$. Laser damage data were then obtained for each sample.

Comparing the results of laser surface damage measurements of the ion bombarded surfaces to the mechanically polished surfaces indicated slight (~10%) improvement for samples polished for 60 and 120 min. No change was detected for a treatment of 30 min, and degradation similar to that described above was seen for the sample bombarded for 180 min.

TABLE V

Surface Damage Thresholds for $LiNbO_3$ Samples at 1.06 μm: Ion Polish versus Abrasive Polish

Sample	Threshold Power Density,[a] GW/cm^2		Number of Thresholds Measured	
	Abrasive Polish	Ion Polish	Abrasive Polished End	Ion Polished End
A	0.86	—	14	—
B	1.95	1.02	7	10
C	0.94	1.06	11	6
D	2.41	2.04	10	10
E	1.22	0.65	9	5

[a]The values are given as the total power divided by the beam area defined as πa^2 where a is the $1/e$ radius for the electric field. The on-axis power densities are twice the values listed in the table.

T997

However, it should be pointed out that lithium niobate damage appears to be limited in all cases by the presence of inclusions. We base this statement on the following:

1. In a number of cases where we attempted to generate entrance surface damage by focusing the laser appropriately we generated bulk damage instead. The bulk damage was characterized by either a series of small fractured sites along the beam or by one or two internal cracks randomly located in the material.

2. The ion polished surfaces were characterized by a number of irregularities not present on the abrasively polished surface which first appeared to be depressions or small craters but subsequently were seen to be small raised mounds. The presence of these irregularities suggests the existence of surface inclusions

that have a different rate of removal in the ion beam than the host material. This type of surface feature is illustrated in the scanning electron micrographs of Fig. 9. For this surface the ion exposure was prolonged in order to emphasize the surface features.

Thus we conclude that the samples of $LiNbO_3$ studied in this program have a sufficiently high density of inclusions that essentially all the damage levels measured so far are not a measure of intrinsic material. Hence the possibility of improving the material quality via ion beam polishing is still open.

2. RF Plasma Conditioning of Lithium Niobate

Late in the program a different treatment was carried out on a single lithium niobate sample with much more promising results. Instead of exposing the sample to a beam of energetic ions, the sample was sputtered in an rf excited oxygen-argon plasma at 300 V bombardment potential for 30 min. The $Ar-O_2$ plasma was operated at a total pressure of 5×10^{-6} Torr with a partial oxygen pressure of 1×10^{-6} Torr.

Laser surface damage measurements were then carried out on the plasma treated surface and compared with data obtained for the mechanically polished surface. For these later measurements on lithium niobate a different measurement technique was used. This technique is probably the most meaningful one for obtaining single pulse damage data on materials whose damage behavior is not well characterized. It consists of firing the laser just once at a particular spot, observing for the occurrence of damage, and moving on to another spot for the next shot. A series of such measurements taken over a range of incident energies give a measure of the probability that the single shot damage threshold lies below a given energy. Because each site is irradiated only once, this type of measurement eliminates possible preconditioning complications (see, for example, Section II-B-3-e) that might occur if the site of interest is exposed to a series of shots at predamage intensities. (Of course, if preconditioning does not occur, as has been established for a number of materials studied, then

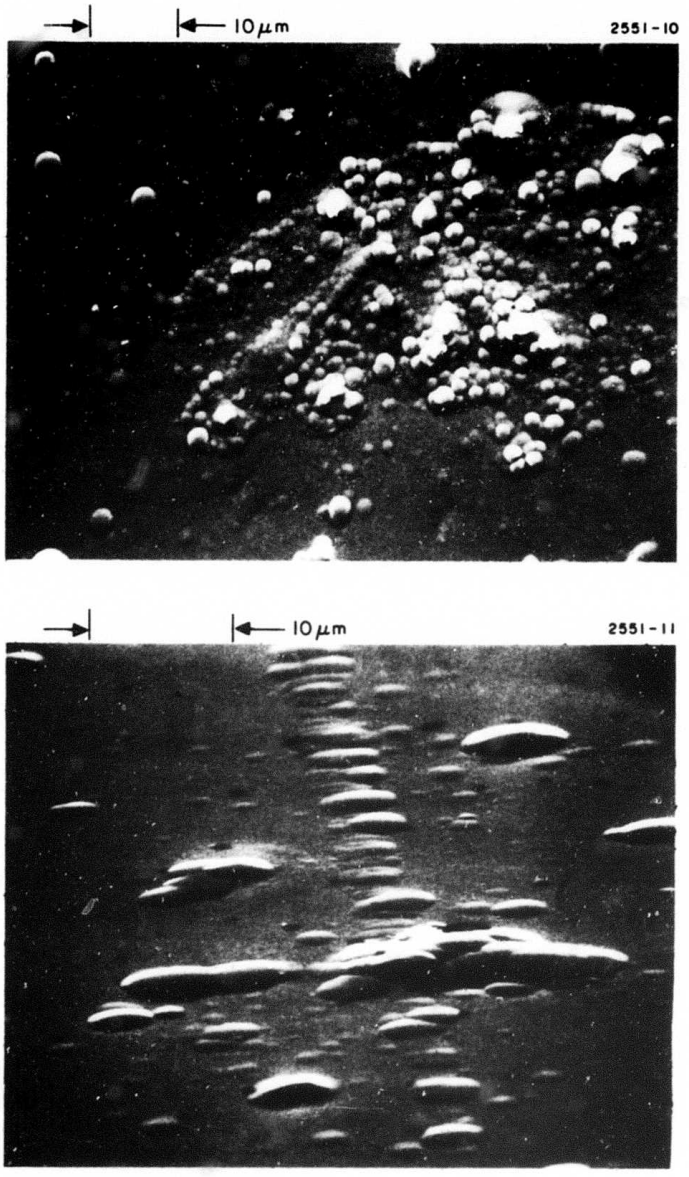

Fig. 9. Scanning electron micrographs of surface features on $LiNbO_3$ after ion beam polishing.

the former technique is adequate.) Because each potential damage site is only exposed once to the incident beam there will be an appreciable fraction of the surface that will not be damaged and hence more sample surface area will be needed using this technique compared with the one first described. Nevertheless, this method shows promise as a means of providing a distribution of single shot damage thresholds over the surface of a sample as well as a measure of damage probability if a threshold is not sharply defined.

While there was a range of intensities at which the surface was found to damage on a single shot, the plasma treated surface had maximum threshold values of 2.5 GW/cm^2 compared with 1.6 GW/cm^2 for the mechanically polished surface. This significant improvement of ~50% indicates that such plasma conditioning should be pursued further.

D. Sapphire Studies at 0.694 μm

1. Surface Damage Threshold Measurements in Ion Beam Polished Sapphire

On an earlier program,[6,12] work was initiated on the use of ion beam polishing as a means of improving the surface damage resistance of optical materials. The main emphasis for these treatments was placed on sapphire. A number of experiments were performed for different conditions of ion polishing, and a distinct improvement was obtained, but the need for further work was evident and some additional experiments have been carried out on this program. These are described below, following a brief discussion of the earlier work.

All the experiments were carried out using the single-mode, Q-switched ruby laser described in Section II-E-3, and the experimental setup described schematically in Fig. 28. The light is focused with a 19-cm focal length lens onto the surface of interest of the sapphire sample whose typical dimensions are 3 in. long by 0.25 in. square cross section.

A typical series of measurements is carried out as follows. The laser is fired at a particular spot on the desired surface at a power below damage threshold. Then the sample is examined through a traveling microscope without disturbing the sample between shots. If no damage is observed, the incident power is increased (by ~10% to 20%), and again the sample is examined. The procedure continues until damage is observed; then the sample is moved and the process repeated on an undamaged spot. Typically 10 to 20 damage thresholds are measured in this way for a given surface.

Abrasively polished samples were used as obtained from the manufacturer (Union Carbide). They were fabricated with the laser finish specifications typical for ruby laser rods. Ion polished samples were exposed after mechanical processing to an Ar^+ beam (7 kV, 300 $\mu A/cm^2$) for periods from 2 to 4 h. The beam strikes the surface at an angle of 20^o from the surface plane. An estimated 200 Å/min is removed from the sapphire surface under these conditions giving a total of about 2.5 to 5 μm of material removed in a given exposure.

Results of the early measurements on abrasively polished samples compared with ion polished samples are shown in Fig. 10. Figure 10(a) shows the exit damage thresholds for the abrasively polished sample. Here, most of the observed damage occurs between 1 GW/cm^2 and 2 GW/cm^2. For the ion polished case (Fig. 10(b)) the exit damage threshold values are distributed over a wide range, but no damage thresholds lower than 2 GW/cm^2 are observed. (The data shown in Fig. 10(b) were obtained from samples that were ion polished for 2 and 4 h. Because no noticeable change in the distribution was observed for the two conditions, the data are presented together in the figure.) The results for entrance surface damage are shown in Fig. 10(c) and (d). For the abrasively polished sample, most of the damage thresholds occur between 1 GW/cm^2 and 2.5 GW/cm^2 with a few higher values observed. For the ion polished case (Fig. 10(d)), we see a few damage thresholds ranging from 2 GW/cm^2 to 9 GW/cm^2 with a large fraction (>50%) occurring above 10 GW/cm^2. The dashed

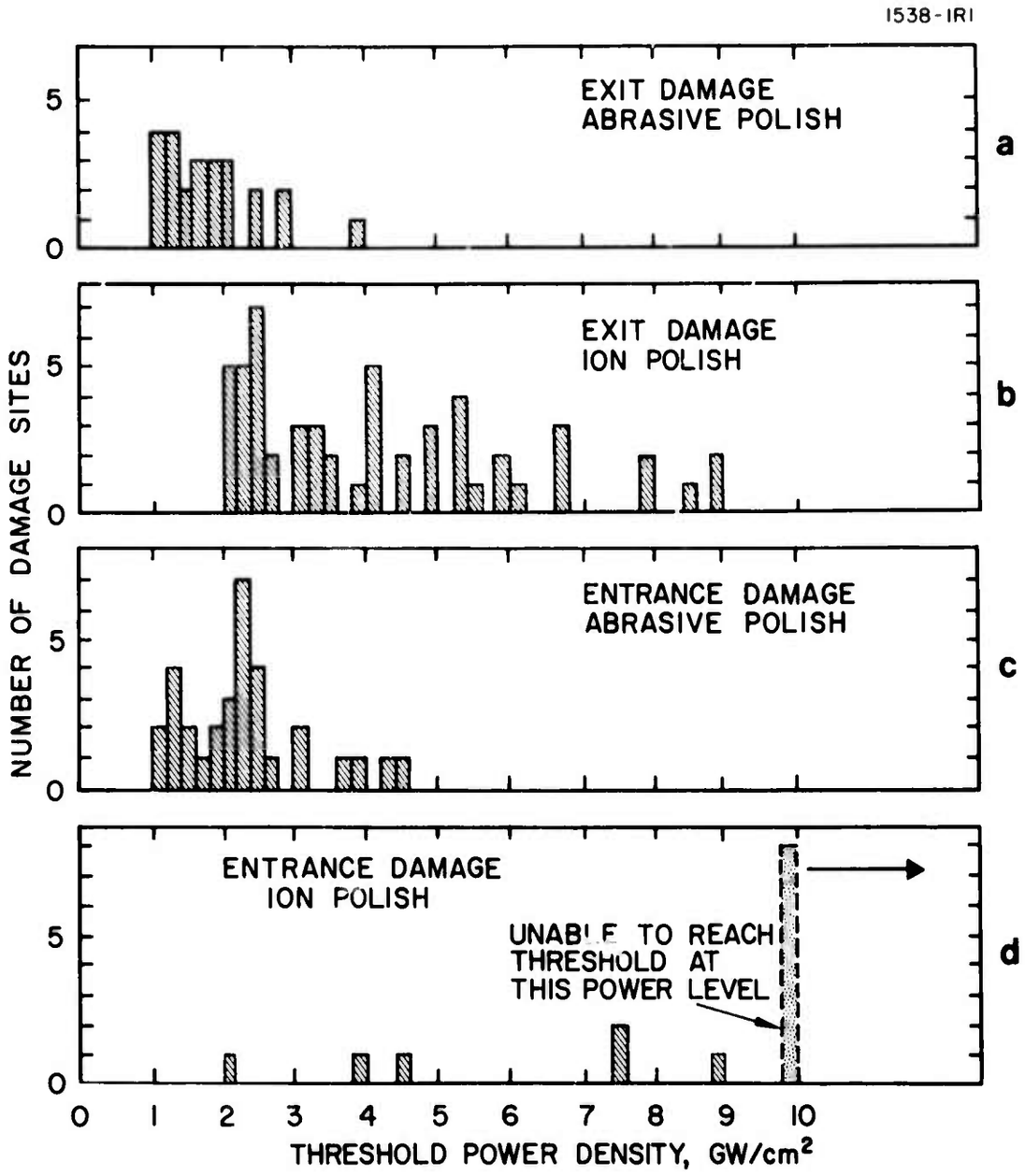

Fig. 10. Histograms of early data comparing damage thresholds for ion polished sapphire to abrasively polished sapphire.

portion of Fig. 10(d) indicates that we were unable to reach damage threshold with the maximum output from our laser under the focusing conditions of our experiment.

One of the main reasons for continuing the study of damage in ion polished sapphire was to obtain additional high-power points for Fig. 10(d). For this we used the ruby amplifier described in Section II-E-3 that was not employed in the earlier measurements. The results of these experiments are shown in Fig. 11(d) with the earlier data for comparison. Here we see damage thresholds that range up to > 20 GW/cm^2. The sample used in these experiments was ion polished for 8 h under the same conditions of ion energy and current as used earlier. The reason for the longer ion beam exposure was to see whether the scatter observed in the earlier threshold data might be reduced somewhat for a longer treatment. We see that this is not the case.

The reason for the large scatter in the threshold data for the ion polished samples compared with that for the abrasively polished samples is not known, although a likely interpretation is that while a distinct improvement in surface quality is gained by ion beam polishing, the improvement is not uniformly distributed over the surface. This improvement in surface quality could be related to either the removal of surface irregularities such as the fine scratches that arise from abrasive polishing, or to the improvement in surface crystallinity as evidenced by x-ray topographs, or both these factors.

Bloembergen[28] has pointed out that the optical electric field strength in the neighborhood of surface features, such as cracks and micropores, can substantially lower the threshold for electron analanche breakdown on the surface of transparent dielectrics. A possible interpretation of the scatter in thresholds for the ion polished samples compared with the abrasively polished sample is that, in the latter case, the surface quality is uniformly poor, resulting in a relatively narrow spread of damage thresholds. For the ion polished surfaces, however, a distinct improvement in quality is attained with regard to

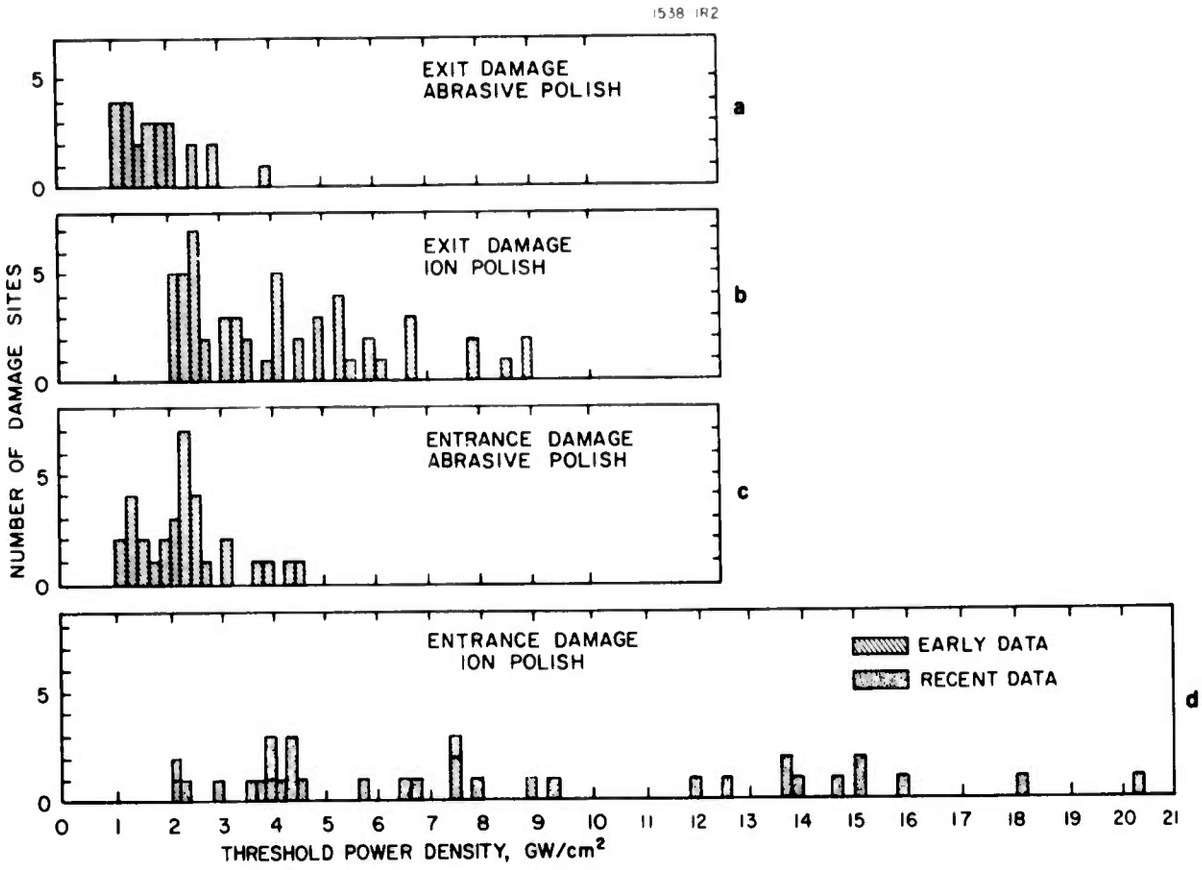

Fig. 11. Histograms of Fig. 10 including new data for entrance damage on ion polished sapphire.

both improved crystallinity and removal of scratches, but this improvement is not uniform over the surface and a broader range of thresholds is observed.

2. Surface Damage for Different Light Polarizations

A series of experiments was performed during this program in which we compared the entrance surface damage threshold of sapphire for linearly and circularly polarized light. The original rationale for performing this comparison arose from the fact that electron avalanche ionization should be sensitive to polarization effects in anisotropic crystals. There was also the curiosity connected with the fact that while two beams of the same intensity, one circularly and one linearly polarized, would have the same rms electric fields, the linearly polarized field would reach a maximum value twice that of the circularly polarized field. Moreover, while the linearly polarized field goes through zero twice for every optical cycle the circularly polarized field is never zero but has a constant amplitude which rotates through an angle of 2π radians in the plane perpendicular to the direction of propagation once per optical cycle. These differences between optical fields suggests that the detailed mechanics for accelerating electrons might be quite different in the two cases, especially when one considers crystalline anisotropy and "lucky" electron collisions.

A series of experiments was carried out measuring surface damage threshold for sapphire for both linearly and circularly polarized light and for different orientations of the crystal axis and optical polarization. The result of these experiments is that the surface damage threshold is independent (within ±8%) of optical polarization or orientation. A discussion of the implications of this result is presented in Section III where mechanisms of optical breakdown are considered.

3. Study of Transmitted, Reflected, and Scattered Laser Light During the Generation of Surface Damage

During this program we have pursued a series of measurements reported in Semiannual Technical Reports Nos. 1 and 2. The purpose of this work is to characterize in detail the laser pulse

with respect to instantaneous intensity, total energy, and spatial properties during the generation of surface damage.

To this end we have examined the temporal shape of both transmitted and reflected pulses as a function of incident power below and above damage threshold for both entrance and exit surfaces. The total integrated pulse energy has been monitored as a function of power for both reflected and transmitted light. In addition to examining the light that is reflected specularly from the sample surface, we also measured the temporal and spatial properties of light that is scattered out of the main reflected beam at moderate angles. For the studies we have used the single mode ruby laser focused on sapphire samples, but it is evident from other cursory observations that the results apply more generally to other materials and optical wavelengths.

a. Integrated Transmission and Reflection of Laser Damage Pulses – In this program we have measured integrated percent transmission and reflection as a function of power for laser pulses. The main motivation for this work has been to determine whether the decrease in transmission of damaging pulses is accompanied by a corresponding increase in reflection as might be expected if the surface plasma density reaches a sufficiently high value.

The experimental setup for monitoring the various pulses is shown in Fig. 12. For the transmission experiments, the output from the detector located after the sample (detector No. 2) is integrated electrically and displayed on one trace of a dual beam oscilloscope (Tektronix 555) while the signal from the detector that monitors the incident energy (detector No. 1) is displayed on the other trace. Appropriate ratios are measured over a range of incident power from below damage threshold to many times above threshold. In a similar manner the percent reflected energy was measured in another set of experiments in which the reflected light that passes back through the focusing lens is monitored by detector No. 3 and displayed on the oscilloscope in place of the transmitted signal. The results of these measurements are shown in Fig. 13.

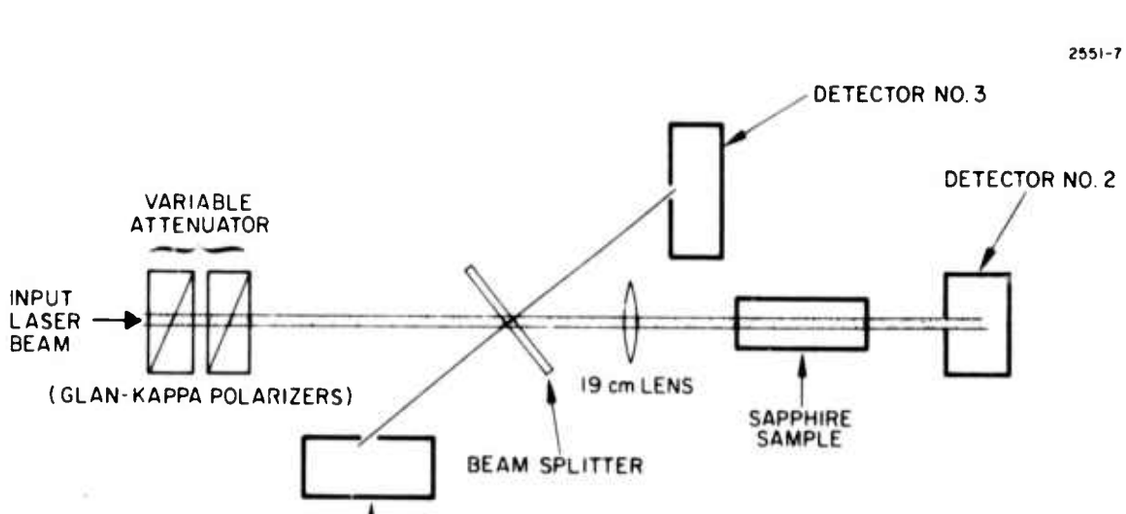

Fig. 12. Experimental setup used in transmission and surface reflection measurements.

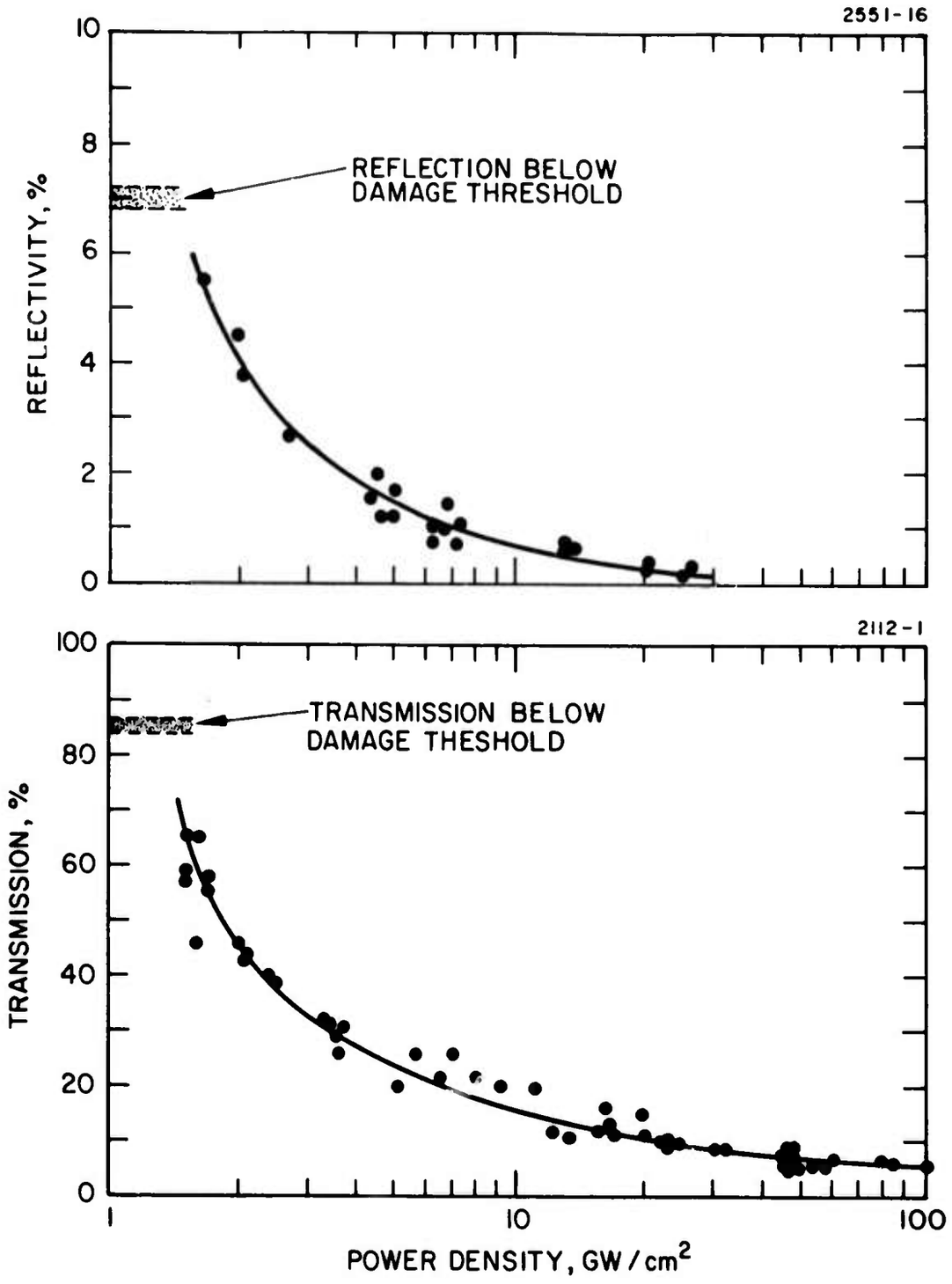

Fig. 13. Integrated transmission and reflectivity of damaging laser pulses as a function of incident power on sapphire surfaces.

The percent transmission data are presented for comparison with the reflectivity data. We see from these curves that both transmission and reflection show a monotonic decrease as the power increases above damage threshold.

b. Temporal Study of Transmitted and Reflected Damaging Pulses – A series of experiments was carried out to simultaneously study the temporal shape of transmitted and reflected pulses as a function of incident power. The purpose of these experiments was twofold: First, to determine whether the sharp drop in transmission at the time of damage formation is accompanied by a corresponding change in reflectivity at the same time, and second, to explore the possibility that some temporal irregularities might be detectable in the back reflected pulse in the absence of catastrophic damage. In essence we were also exploring for clues for precatastrophic damage information.

As we will see later, examination of the back-reflected light showed no indication of precatastrophic behavior, but there was evidence for such behavior when small-angle backscattering away from the directly back-reflected beam was studied.

For these experiments the outputs from detectors 2 and 3 in Fig. 12 were individually displayed on separate Tektronix 519 oscilloscopes. The use of either line filters or Wratten No. 70 red filters assured that only laser light was detected. Both oscilloscopes were externally triggered by a pulse taken fron an additional biplanar photodiode that is normally used to monitor the oscillator output. This external triggering scheme ensured that the two oscilloscopes are triggered at the same time (within less than 1 nsec). In this way variations in pulse shape for transmitted and incident light can be temporally related even though they are separately recorded.

For each of the oscillographs recorded, a double exposure was taken. In the first trace, we recorded the signals when the laser was fired at the sample with the focusing lens removed from the optical path. For the second trace, the lens was appropriately positioned so

that the light was focused on the surface of interest and the laser was fired again. The reproducibility of the ruby laser-amplifier combination is such that in each case (i.e., with lens and without lens) the total energy incident on the sample was the same (within ~5%). Hence, in the absence of damage, each transmitted and reflected oscilloscope photograph shows a pair of traces of the same shape and amplitude. When damage occurred the temporal variations of the damaging pulse can be compared relative to the nondamaging pulse, both with respect to transmitted light and reflected light.

Experiments of this type were carried out in detail for both entrance and exit surface damage on sapphire, and the results of representative shots for different incident laser power are shown in Figs. 14 and 15. Because of the difficulty in reproducing high speed oscilloscope photographs, tracings of these photographs are shown. After a great deal of difficulty it was possible to obtain reliable triggering and to eliminate all influence of stray scattered light on the recorded signals.

The following features should be pointed out concerning the traces in the figures under discussion:

- The back-reflected pulse cuts off at the same time as the transmitted pulse.
- Most temporal irregularities in the transmitted pulse are duplicated in the reflected pulse.
- The back-reflected intensity for a damaging pulse is always less than or equal to that of the reference pulse. That is, the specular reflectivity of the interface during the occurrence of damage is always less than that of the undamaged interface.

Because of the lens diameter (1 in.) and distance from the sample surface (20.7 cm) the total amount of reflected light collected in the experiments described above would have spanned a maximum half angle of 3.5°.

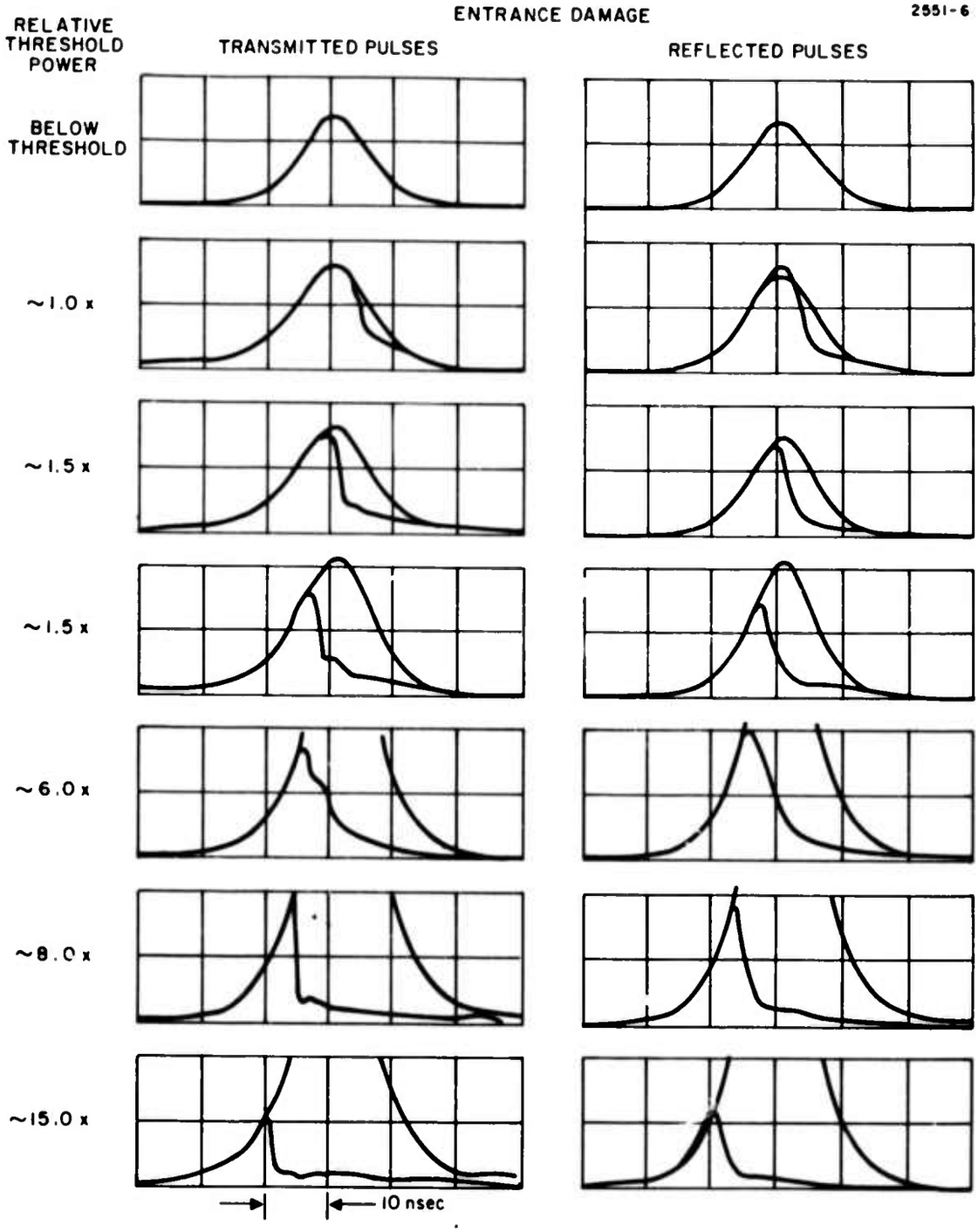

Fig. 14. Temporal shapes of transmitted and reflected pulses for different powers relative to threshold for entrance damage.

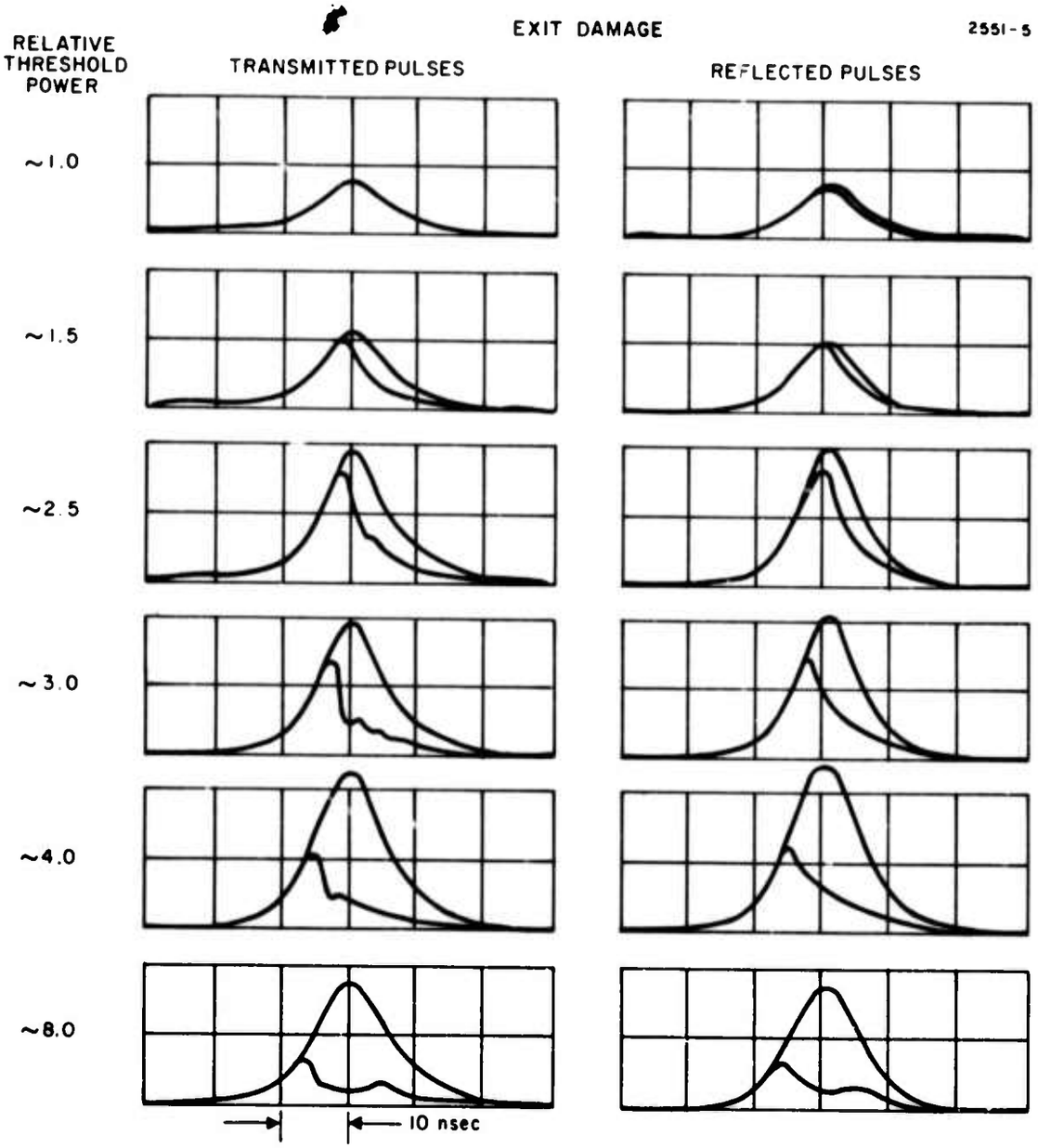

Fig. 15. Temporal shapes of transmitted and reflected pulses for different powers relative to threshold for exit damage.

c. Measurements of Backscattered Laser Light From the Surface During Damage – Since both the transmitted and reflected pulses show a sharp decrease in intensity following the creation of damage, one might be inclined to attribute the loss of light to absorption by the damaged region and/or surface plasma. However, there is also the possibility that an appreciable amount of the laser light is scattered out of the forward and back direction as well as absorbed.

A measurement of the amount of scattered light would require the means for collecting and measuring the light scattered over all directions or a knowledge of the scattering distribution and subsequent sampling of the light over a particular solid angle. Measurements of this type were not carried out in our experiments but a few experiments were conducted that were directed toward determining the temporal behavior of scattered light. Again, the purposes were: (1) to explore the possibility that an appreciable amount of light might be scattered out of the main beam, (2) to obtain a temporal correlation between the scattered light and transmitted or specularly reflected light, and (3) to explore the possibility that some indication of precatastrophic damage might be found in the temporal characteristics of the scattered light.

The experimental setup used for these experiments is shown in Fig. 16. It is similar to the previous setup, except that a white card (3 in. sq) with an aperture was placed approximately halfway between the focusing lens and the sample. Detector No. 3 was placed to monitor the diffuse laser light scattered back from the sample surface onto the white card. The aperture diameter (6.5 mm) was substantially larger than the convergent beam diameter (1.7 mm) at the point where it passed through the hole in the card.

The experimental data were obtained in a similar way that the previously described data were taken; the laser was fired once with the lens removed and the second time with the lens placed appropriately in the beam, both pulses being recorded on the same oscilloscope film.

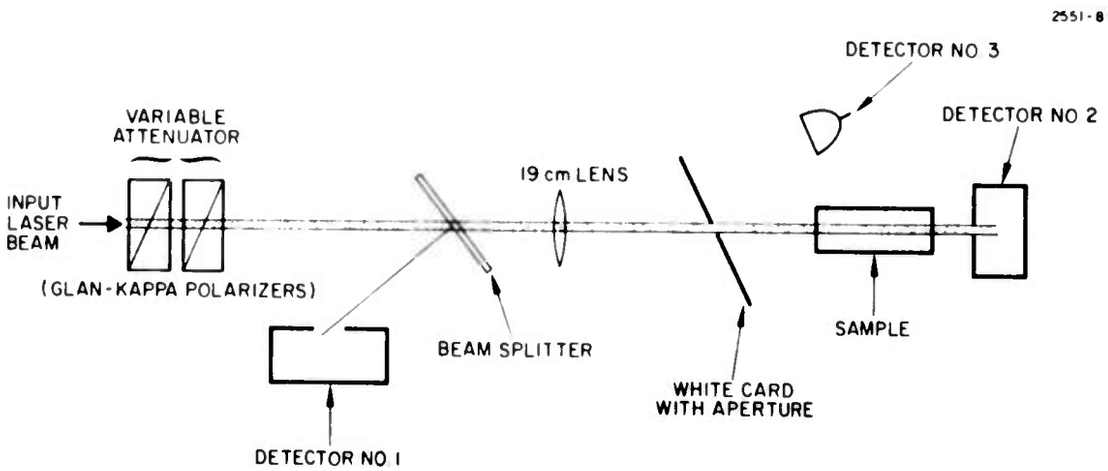

Fig. 16. Experimental setup used in backscattering measurements.

The results of a number of these experiments are illustrated in Fig. 17. Here the data are displayed differently than before in that the scattered pulse has been inverted relative to the transmitted pulse so that the temporal relationship can be more easily seen.

The general qualitative features seen in these traces are:

- The scattered light for damaging pulses is characterized by a sharply rising spike followed by a more slowly decaying tail.
- The peak of the scattered spike occurs at the same time that the transmitted pulse begins its sharp cutoff.
- The scattered intensity begins to rise from its background level before the transmitted pulse shows any appreciable irregularity.
- In cases where very slight damage occurs so that the transmitted pulse shows little or no temporal irregularity, there is still an appreciable temporal irregularity in the scattered light.

The sensitivity of the backscattered amplitude shown in the above experiments indicates that this type of monitoring is a more sensitive indication of surface damage than examination of either the transmitted or the specularly reflected light. Moreover, the fact that the backscattered light begins to rise in intensity relative to the background before the transmitted light shows signs of cutoff suggests that some evidence for precatastrophic damage may be indicated from this kind of measurement.

d. Precatastrophic Damage Experiments – Tentative evidence for precatastrophic damage indications were seen in a few instances in the absence of damage where the scattered light showed a definite irregularity compared with the background pulse. In these cases the transmitted pulses were essentially identical with or without the focusing lens in place, whereas the backscattered pulse with the lens in place had a different shape than the pulse observed with the lens removed.

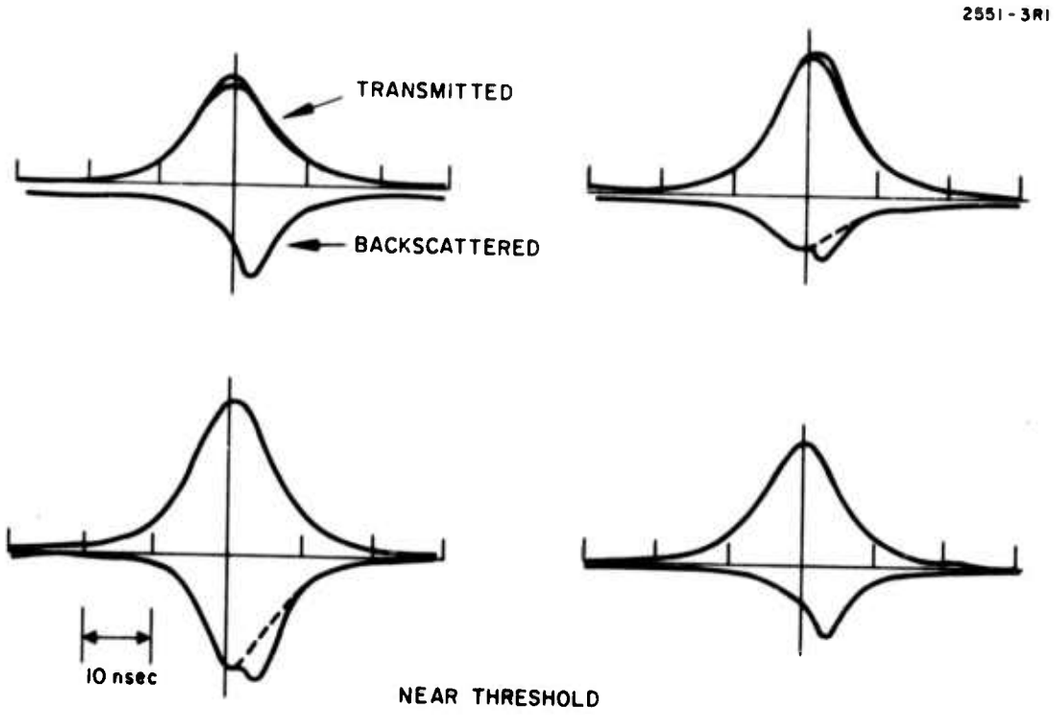

Fig. 17(a). Temporal profiles of laser pulses transmitted through and backscattered by sapphire samples at different powers relative to entrance surface damage threshold.

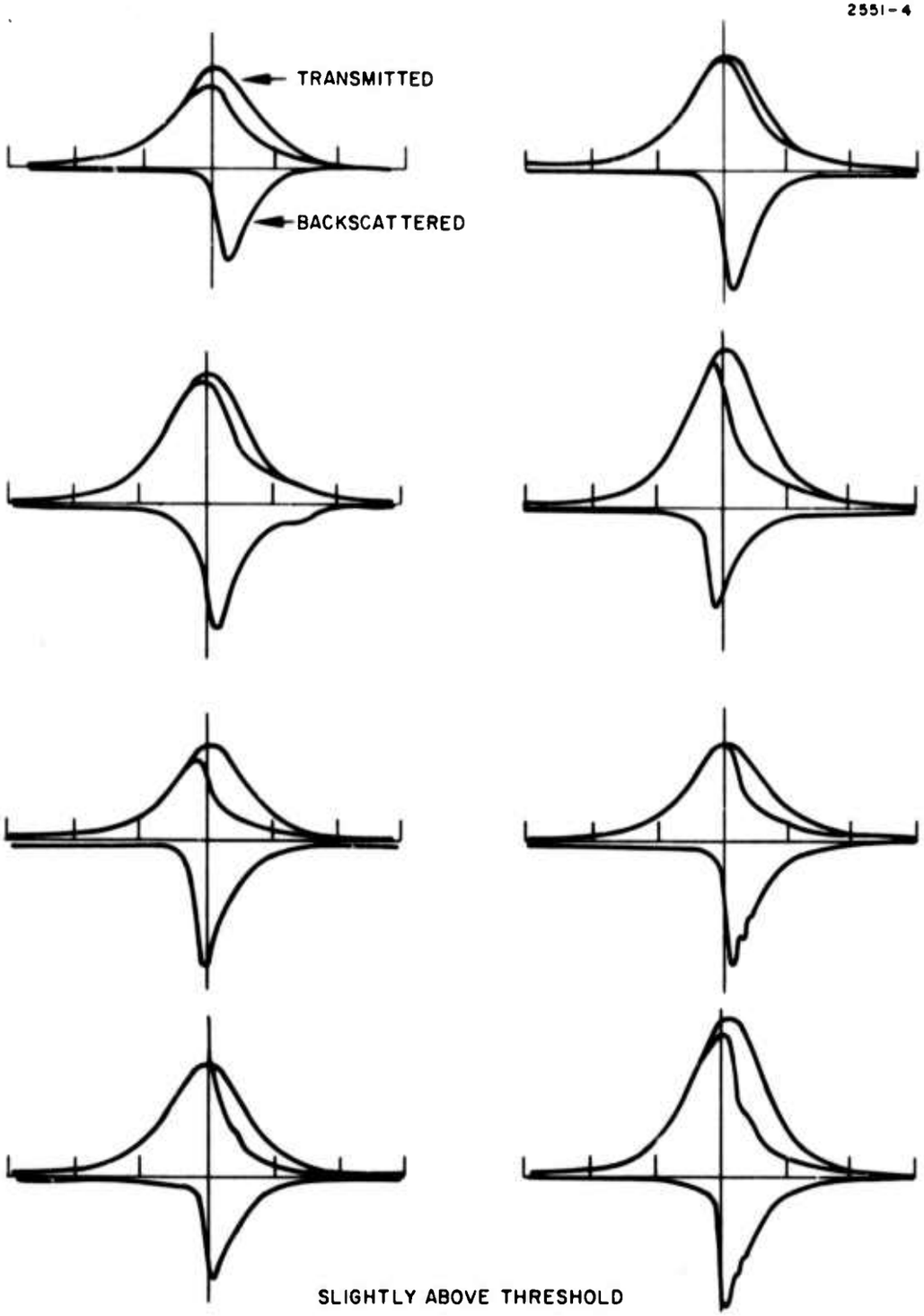

Fig. 17(b). Continued.

Examples of this behavior are shown in Fig. 18. We see that the scattered pulse with the lens in place is different in shape from the one in which the lens is removed. In these examples the laser power incident on the surface was very close to the value where damage occurred but not sufficiently large to produce any detectable damage on that particular shot. All the pulses in the examples shown were followed by damage producing pulses of slightly higher energy. Because of the detector sensitivity, it is difficult to obtain large signals at these levels of illumination.

The amplitude of the backscattered signal for the nondamaging reference pulse (dashed traces in Figs. 17 and 18) depends on the size of the aperture chosen and the alignment of the sample. Sometimes the unfocused beam was not reflected completely through the hole in the white card and the reference signal would be correspondingly larger than that obtained for normal incidence. Since the background pulse in these experiments is one in which the lens is removed from the system, the diameter of the beam in passing through the 6.5 mm aperture is different in the two cases. (The diameter of the focused beam at the $1/e^2$ intensity points is 1.7 mm and that for the unfocused beam is ~4 mm.) Also the fact that the reference pulse is not focused means that it strikes a larger surface area (and hence may be scattered differently) raising some question as to the validity of comparing the pairs of pulses on the double exposure oscilloscope pictures.

In later experiments we changed the procedure for taking data so that the reference pulse could be employed more meaningfully. For these experiments the focusing lens was left in place for both shots obtained on the double exposure oscillogram. For the first shot recorded (the low power nondamaging reference trace) a Wratten neutral density filter ND 0.3 was placed in the laser beam just past the Glan-Kappa polarizers (Fig. 16). The laser intensity in this part of the beam was never high enough at the levels we used to cause any bleaching or damaging of the filter and the ~2x attenuation was reproducibly obtained. For the second shot of the double exposure oscillogram (the high power, potentially damaging shot) the ND 0.3 filter was

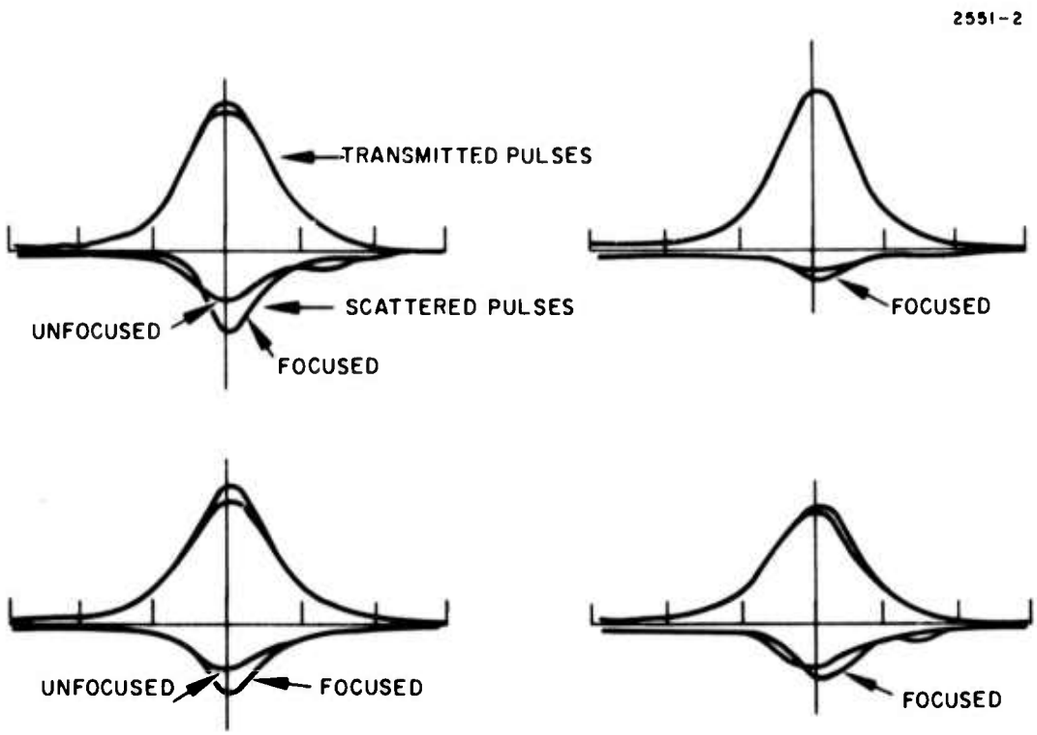

Fig. 18. Backscattered pulses compared with transmitted pulses below damage threshold showing temporal irregularities in the backscattered pulse.

removed from the main beam and placed in front of detector No. 3 (the one that monitors scattered light) and another filter with the same attenuation as separately measured was placed in front of detector No. 2 (the one that monitors transmitted light). In this way signals seen by detectors 2 and 3 would be the same for both pulses as long as the sample behaved in a linear fashion. This was confirmed in detail for a series of pairs of pulses, neither of which was intense enough to create damage. The result was a number of double exposure oscillograms in which both pulses were essentially superimposed.

Using the above technique, we carried out a detailed series of experiments for different incident laser powers. We essentially confirmed the results obtained earlier using focused and unfocused beams and satisfied ourselves that the reference beam traces as depicted in Figs. 17 and 18 are, in fact, valid comparison traces.

Most of the measurements performed using the above described method were directed toward exploring whether signs of precursory damage could be detected reliably and reproducibly by monitoring the backscattered temporal profile. Occasionally (less than 5% of the time), we would obtain traces similar to those illustrated in Fig. 18 where the transmitted pulse showed no change from the reference pulse but where the backscattered pulse was distinctly different from its reference pulse and where there was neither a visible spark of any kind nor any detectable surface damage on subsequent microscopic examination. Possible explanations for this behavior are local heating causing a slight surface curvature that could deflect the beam temporarily off axis or the formation of a microscopic surface plasma that could scatter light. Another possibility is the chance encounter of a scattering dust particle that happens to be illuminated somewhere between the screen and the sample surface.

Of course, all this is mere speculation; the practical result of these backscattering measurements is that while definite precursory effects are observed in the absence of catastrophic damage, they are too subtle to be easily characterized and at this point do not indicate a practical reproducible means for nondestructive damage threshold determination.

e. Spatial Properties of Backscattered Light From Damaging Pulses – The fact that a measurable amount of light is scattered out of the specularly reflected beam for damaging pulses led to the question concerning its spatial distribution. To this end an experiment was carried out, as illustrated in Fig. 19, where the specularly reflected light was allowed to strike a photographic film (Polaroid Type 47). In addition to photographing the reflected beam as a function of incident total energy, the spot was photographed for different diameter apertures placed in the beam between the lens and the sample. In this way angular information could be obtained for some of the off-axis features.

Qualitative features of these beam profiles are shown in Figs. 20 and 21. At low powers a smooth circular spot is seen that remains essentially unchanged when damage threshold is reached and even substantially above damage threshold (~2x). At higher powers (above twice threshold) signs of off-axis features begin to appear and an increasing amount of light is detected in the form of irregular rings and bright spots.

The angular extent over which the pattern is detected was measured by varing the size of the aperture between the lens and the sample. It was found that an aperture diameter between 5.5 and 7 mm was the smallest that could be used to give the same pattern as obtained with no aperture in the system (Fig. 21). (The effective limiting aperture caused by the lens would be 12 mm at that position.) Hence the off-axis features in the photographs extend over a half angle of from 1.5° to 2°.

It should be pointed out here that the measurements of "specularly" reflected light discussed earlier included the light that is shown in the photographs of Figs. 20 and 21. Because of the setup used in those experiments, the angular acceptance of the detected light was on the order of 3° half-angle. Hence, even though a detectable amount of light is scattered out of the specular beam, the total amount of light collected over the 3° half angle shows the general decrease with power above damage threshold.

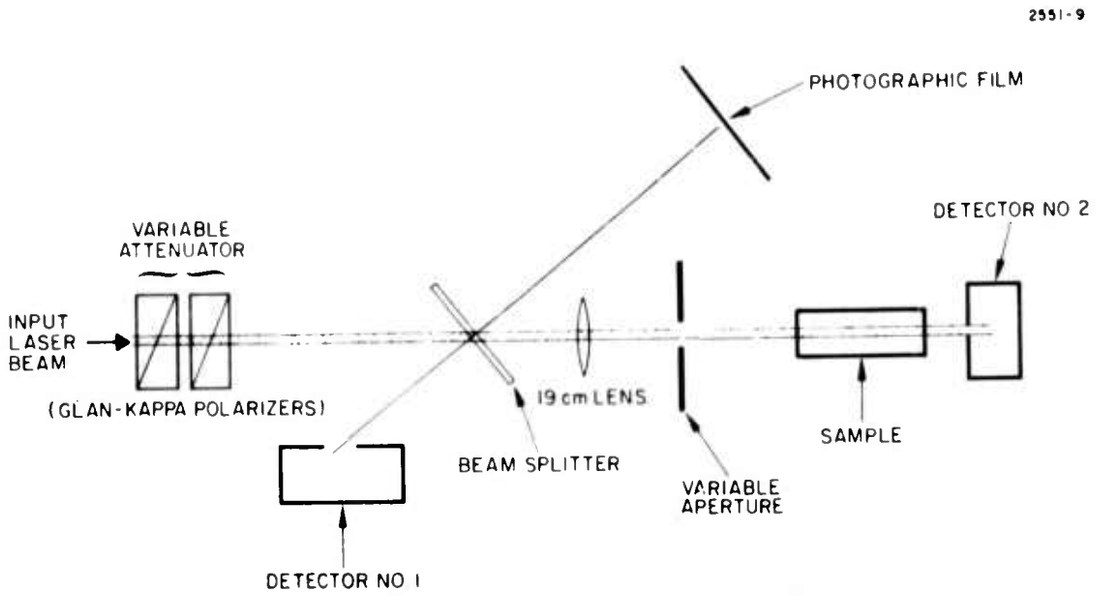

Fig. 19. Experimental setup for photographing spatial features of specularly reflected light.

2551-13

Fig. 20.
Photographs of back-reflected beam for increasing laser power above damage threshold (from 1 to 10x).

2551-12

APERTURE DIA, mm

Fig. 21.
Photographs of back-reflected beam for different aperture sizes between lens and sample. Constant laser power for each shot ∿10x threshold.

Along the same line of discussion, the temporal spikes detected in the off-axis scattering experiments (Fig. 17) were seen to occur at half angles larger than 2°; none of the light detected in those experiments was of sufficient intensity to be recorded on the beam photographs.

f. Summary of Pulse Temporal and Spatial Experiments -- The results of the above measurements can be summarized as follows:

1. The damaging pulse shows a sharp temporal cutoff both in transmission and reflection for light collected over a cone of 3.5° half angle.

2. Photographs of the back-reflected light show that a considerable amount of this light is scattered out of the main beam at small angles (less than 2°) in the form of bright spots and diffuse rings.

3. In addition to the small angle backscatter seen in the photographs, an appreciable amount of light is scattered back at larger angles that is not seen photographically.

4. The light scattered back at larger angles (within a 23° half-angle cone) shows a sharp temporal spike at the time the transmitted light and specularly reflected light cuts off.

5. Tentative evidence indicates the possibility that precatastrophic effects can be explored through observation of this large angle backscattered component.

6. Although it is almost certain that the damaged surface site and associated plasmas absorb a measurable amount of the incident pulse, it is not possible to obtain an accurate measure of the light absorbed during damage without integrating all the scattered light.

g. Brewster Angle Reflectivity as a Function of Incident Intensity – During the latter stages of our backscattering measurements in search of precursory damage phenomena we decided to explore for nonlinearities in the reflectivity at Brewster's angle. The rationale for this type of experiment was based on the fact that the

nonzero value of the reflection coefficient for real dielectrics at Brewster's angle is attributed to slight residual absorption and that if some subtle surface disturbance were occurring prior to catastrophic damage, it might be detectable as a power dependence in this reflectivity. To explore this possibility we set up an experiment shown schematically in Fig. 22 in which the incident energy, the Brewster reflected, and the transmitted light were all monitored. The signals from detectors 2 and 3 were displayed on Tektronix 519 and 7904 oscilloscopes so that we could look for temporal irregularities in the Brewster reflected light compared with the transmitted light. Reference pulses in the double exposure oscillograms were obtained in a similar manner to that described in Section II-D-3-d. For these experiments the light from the ruby laser was focused on a sapphire sample using the 19 cm lens. Figure 23 shows a series of double exposure oscilloscope traces comparing the transmitted and Brewster reflected pulses over a range of powers from the onset of damage to about 3.5 times damage threshold.

The results of these experiments are summarized below:

- Over a range of incident power from 1/10 damage threshold up to damage threshold the total energy reflected at Brewster's angle is a linear function of input energy.

- Over the range of incident powers below damage threshold the temporal shapes of the Brewster reflected pulse and the transmitted pulse are identical showing no evidence for precatastrophic damage.

- The Brewster reflected light shows a cutoff similar to that of back-reflected light (Figs. 14 and 15) but occurring slightly later than the cutoff in transmission.

- While the transmitted and back-reflected pulses remain at a low level from the time of cutoff throughout the remainder of the pulse, the Brewster reflected pulses return to a "normal" level before the pulse ends (i.e., the Brewster and reference traces meet again before the end of the pulse while the transmitted pulse remains cut off).

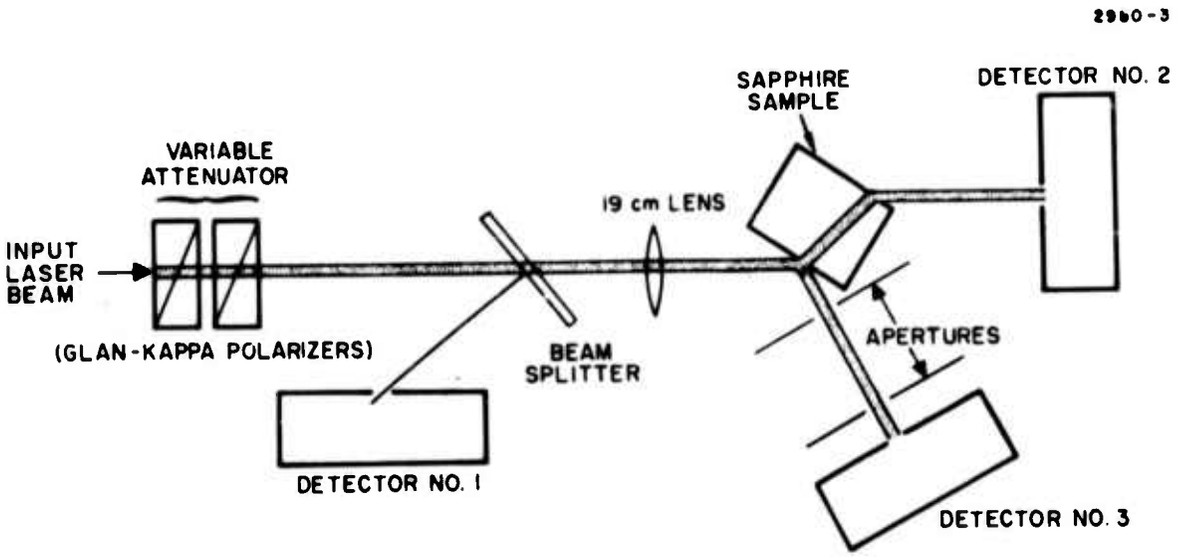

Fig. 22. Experimental setup used in transmission and Brewster reflection measurements.

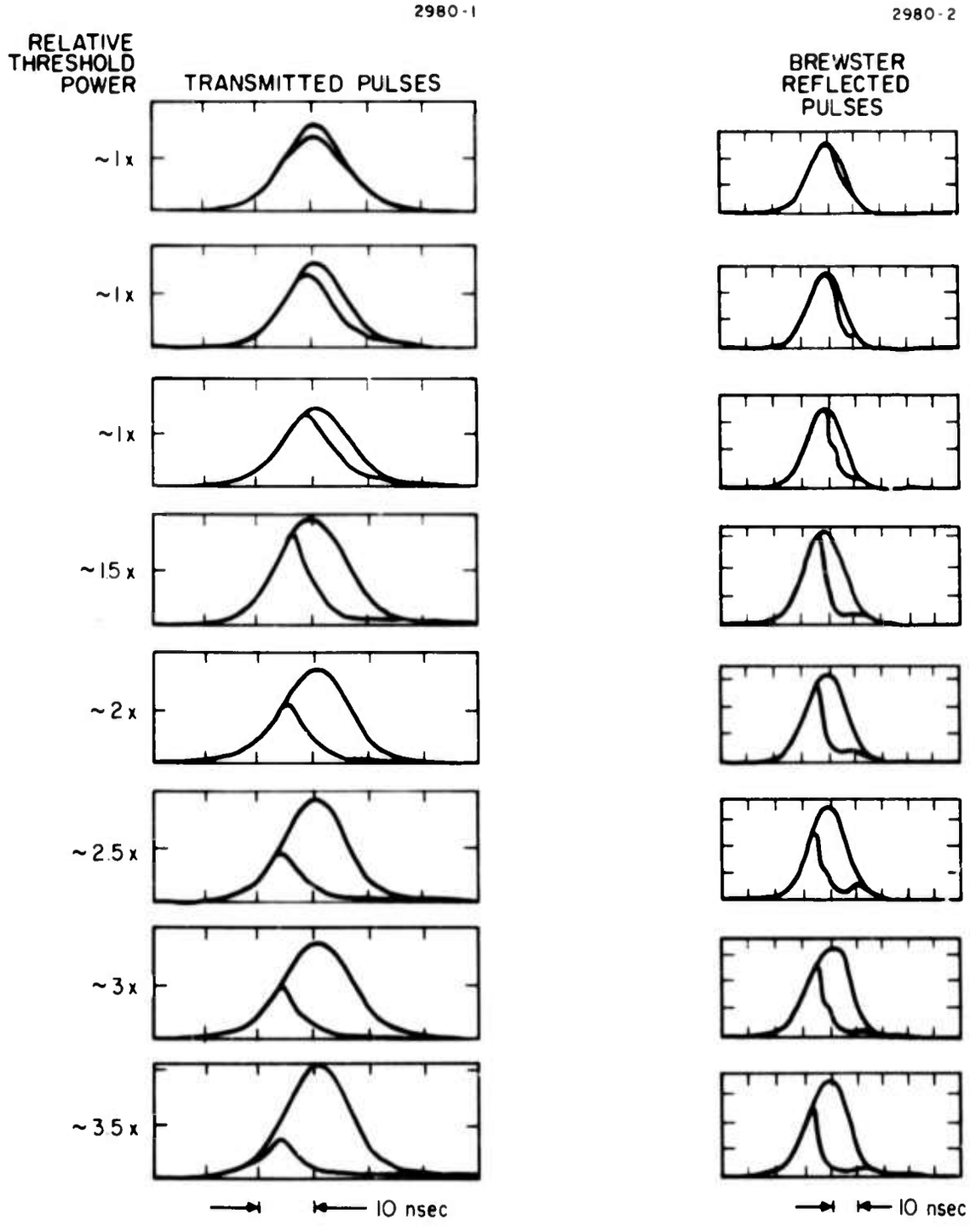

Fig. 23. Temporal shapes of transmitted and Brewster reflected pulses for different powers relative to damage threshold.

The fact that the Brewster reflectivity is independent of intensity below damage threshold indicates that there is little change in surface absorption during the time of irradiation before damage occurs. Hence, this type of measurement apparently is not a sensitive means for exploring precursory damage phenomena. It is somewhat surprising that the Brewster signal is lower than the reference pulse during damage generation. One would expect that if the surface absorption were to increase at the time of damage (which it apparently does) the Brewster signal would increase as well. There are probably a number of effects contributing to the observed behavior and further clarification can only be obtained by other measurements. Possible explanation for the decrease in the Brewster signal are absorption and scattering in the surface plasma by an amount that exceeds the expected increase in reflectivity and/or possible steering or focusing effects that would cause the beam to be temporarily cut off by the apertures used to eliminate background scatter. These possibilities can only be explored by further study of the spatial and temporal characteristics of the Brewster reflected beam.

E. Lasers Used in Damage Studies

1. High-Power Nd:YAG Laser

The high-power Nd:YAG laser (as schematically illustrated in Fig. 24) is pulse-excited by a Kr-arc pump lamp and electro-optically Q-switched. It has the capability of being triggered externally from single-shot operation to maximum repetition rate of 10 pps or internally triggered at 10 pps. The Nd:YAG rod is 0.25 in. diameter by 2 in. long, pumped by the 2-in. arc length Kr lamp in a close coupling configuration. The output coupler is a flat 47% transmission mirror, and the high reflector (HR) used is a 53-cm radius-of-curvature mirror. To achieve single transverse mode control, the resonator cavity is internally apertured by a 2-mm diameter pinhole placed 14 cm from the HR mirror. The laser resonator is 52 cm in length.

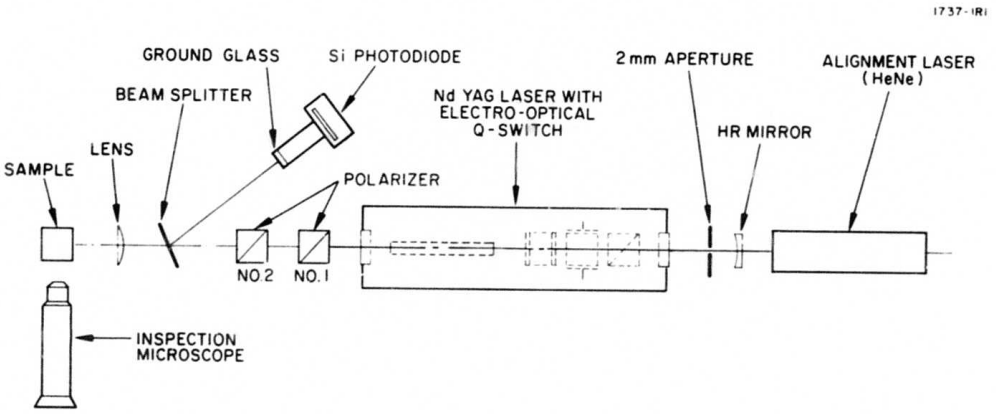

Fig. 24. Experimental setup for damage experiments using high-power Nd:YAG laser.

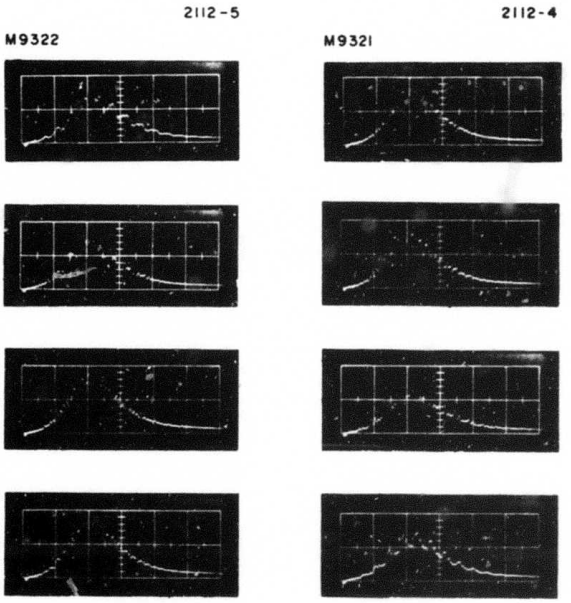

Fig. 25.
Typical oscilloscope traces of output from eight consecutive shots of high-power Nd:YAG laser. Sweep rate is 10 nsec/div.

At full output (i.e., no transverse mode control), the output energy is approximately 100 mJ/pulse with about a 20-nsec pulsewidth. However, when apertured to produce the desired transverse mode profile, the output energy is reduced to about 7 mJ/pulse with an 18.5-nsec pulsewidth. For single-shot operation, there exists a ±3% amplitude fluctuation in the pulse height from shot to shot. When operated at 10 pps, the amplitude fluctuation disappears and the output is very stable. Since no longitudinal mode control is employed, the pulse is temporally modulated with amplitude and frequency varying somewhat from shot to shot. Oscilloscope traces illustrating this modulation for a series of eight consecutive shots are shown in Fig. 25.

2. Low-Power Nd:YAG Laser

The low power Nd:YAG laser (as schematically shown in Fig. 26 is continuously pumped by a Kr-arc lamp and acousto-optically Q-switched. It has the capability of being operated continuously, single pulsed, or repetitively Q-switched at rates up to 50 kHz. The pump cavity utilizes an elliptical 2-in. long cylinder with walls coated with evaporated gold. The Nd:YAG rod is 0.25 in. diameter by 2 in. long, whereas the Kr-arc lamp discharge is 2 in. long with a 4-mm bore diameter.

The resonator cavity is formed by two 1-m radius-of-curvature mirrors separated by a distance of 65 cm. For the experiments, a 4.2% transmission output mirror was used. An internal aperture of variable diameter provided the transverse mode control. By decreasing the aperture size, the TEM_{00} output mode of the laser can be obtained by progressively eliminating the higher order transverse modes. The TEM_{00} is then selected with the collapse of the degenerate TEM_{10} mode. An ultraviolet excited IR phosphor screen is utilized for visual selection of the TEM_{00} mode.

At full power, multimode output of 54 W is obtainable using a single 2.5-kW Kr-arc lamp. However, because of the well-known thermally induced birefringence of the Nd:YAG rod, the TEM_{00} output was drastically reduced to approximately 1.5 W maximum. (No attempt

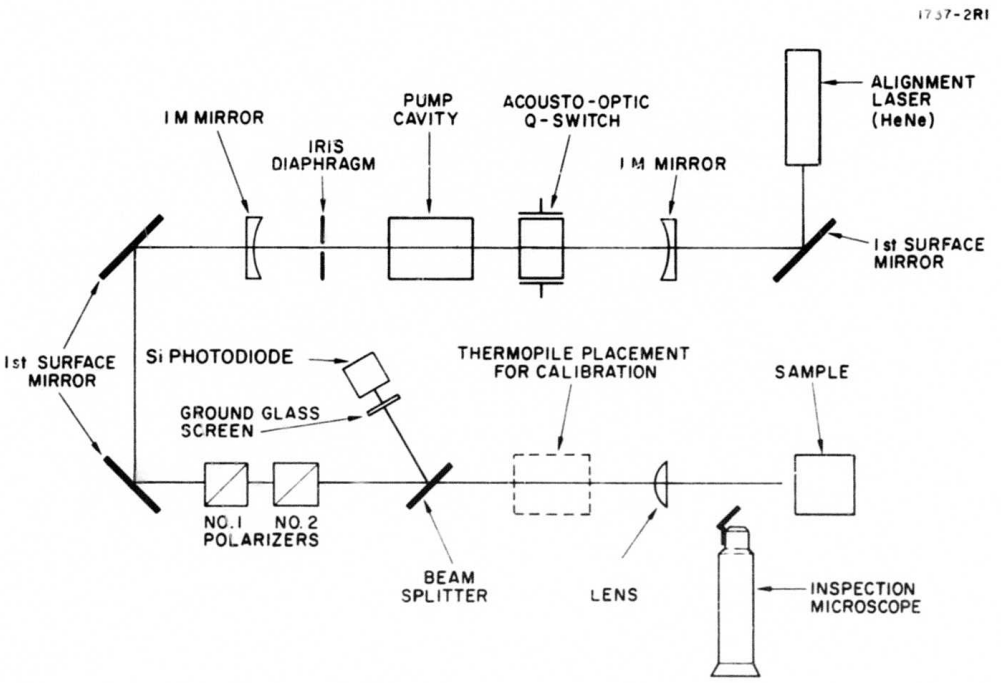

Fig. 26. Experimental setup for damage experiments using the low-power Nd:YAG laser.

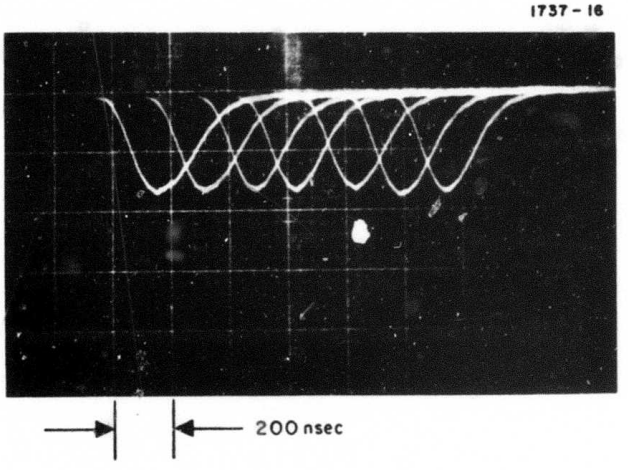

Fig. 27.
Oscilloscope traces showing output of low-power Nd:YAG laser for seven consecutive shots.

was made to compensate the induced birefringence.) This resulted in peak powers of about 1 kW at low repetition rates (< 500 pps). The peak power decreased monotically for high repetition rates. Pulse-widths of between 180 to 300 nsec resulted, depending on the repetition rate used. Amplitude stability was ~±3% when a number of single shots showing the typical reproducibility for this laser is shown in Fig. 27.

3. High-Power Q-Switched Ruby Laser

The experimental setup is shown in Fig. 28. The oscillator employs a 4 in. long by 0.25 in. diameter ruby, pumped by two linear lamps in a double elliptical pump cavity. The ruby crystal is water cooled by a closed cycle refrigeration system maintained at $0^{\circ}C$. The high reflectivity mirror is coated with a 99+% reflectivity high-field damage coating from Perkin Elmer Corporation. Q-switching is accomplished with a solution of cryptocyanine in methanol in a 1-mm path length cell whose transmission is 30% at 6943 Å. The 2-mm aperture allows oscillation in the TEM_{00} mode.

The temperature controlled ($34^{\circ}C$) resonant reflector that was designed to optimize longitudinal mode control consists of two quartz etalons and a quartz spacer, whose combined effect is to enhance cavity modes separated by 2 cm^{-1} and to discriminate against intermediate modes.

Portions of the laser beam are split off in various ways (see Fig. 28), so that the power output, near- and far-field patterns, and Fabry-Perot patterns can be monitored for each shot. An oscilloscope trace of a typical output pulse for this laser is shown in Fig. 29.

The water-cooled amplifier ruby is 6 in. long by 0.5 in. diameter, with one end wedged relative to the other by about 0.5°. The input end of the amplifier rod is antireflection coated to minimize the chances of oscillation within the amplifier itself. The ruby rod is closely coupled to a helical flashlamp, which is pumped with power supply capable of delivering 8 kJ in a 3-msec pulse. The power supply

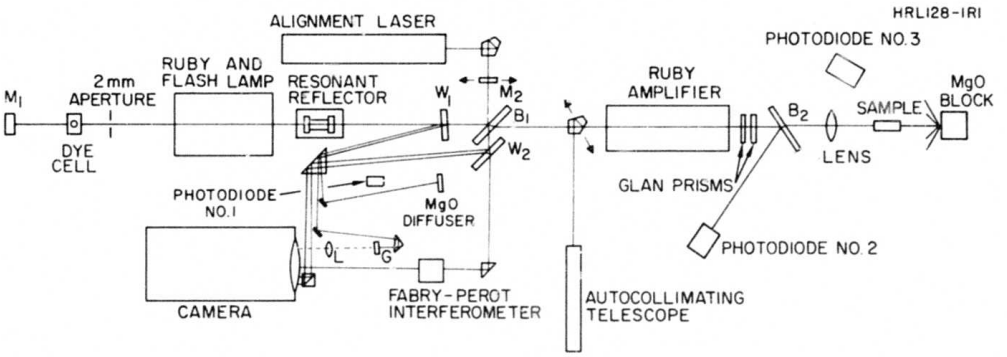

Fig. 28. Experimental setup for damage experiments using single mode ruby laser and amplifier.

HRL 265-5

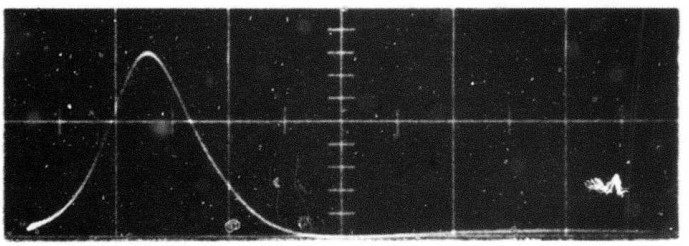

Fig. 29.
Oscilloscope trace showing ruby laser output. Sweep rate is 20 nsec/div.

employs a pulse shaping network of 20 sections, each section pumping for 150 μsec. The maximum gain obtained with the amplifier is about 10 dB.

Table VI compares the characteristics of the three lasers utilized for this program.

TABLE VI

Characteristics of Lasers Used on Program

Properties	High Power Nd: YAG	Low Power Nd: YAG	High Power Ruby Laser
Wavelength	1.06 μm	1.06 μm	0.694 μm
Operating Characteristics	Single shot to 10 pps	Single shot to 50,000 pps or cw	Single shot
Mode Properties	TEM_{00}	TEM_{00}	TEM_{00}
Peak Power (Pulsed Mode)	300 kW	1 kW	~1MW
Energy per Pulse	~6 mJ	~0.25 mJ	~15 mJ
Pulse Width (FWHM)	18.5 nsec	260 to 300 nsec	~20 nsec
Average Single Mode cw Power	--	1.5 W	--

F. Beam Diagnostics and Power Calibrations

1. Beam Diagnostics at 1.06 μm

Details of the beam spot sizes were determined by measuring the diameter of burn spots on unexposed developed Polaroid film for known incident powers ranging from the burn threshold to the maximum power available from the laser. The measurements were made for the two Nd:YAG lasers employed in this program. For the Nd:YAG lasers, spot size was determined at the position of the

entrance surface of the proustite samples that were studied. This position is slightly upstream from the waist of the beam as it is focused by the 11-cm lens.

For each laser, about 40 shots were taken for which burn spots were measured. The diameters of the burn spots were measured using an optical microscope with a calibrated reticle at 200x magnification. The technique was found to be well suited to this sort of measurement. It was found that the burn spots are extremely well defined: the boundary between the burned and unburned regions of the film is very sharp. Examples of burn spots are shown in Fig. 30. The validity of this technique is based on the assumption that the film possesses a sharp burn threshold, and that the diameter of a given burn spot is equal to the beam diameter at which the intensity (or energy density) equals the burn threshold.

The following expression would then apply for a gaussian beam:

$$I_t = I_o \exp (- d_t^2/4a^2) \qquad (2)$$

where I_o is the peak intensity, I_t is the intensity at burn threshold, d_t is the diameter of the burn spot, and a is the characteristic 1/e radius for the intensity.

Taking logarithms we have

$$\ln I_o = d^2/4a^2 + \ln I_t \qquad (3)$$

From eq. (3) we see that a semilog plot of peak power versus the square of the burn spot diameter should give a straight line with slope equal to $1/4a^2$ and intercept equal to $\ln I_t$ for a gaussian beam profile. Deviations from gaussian behavior will be evidenced as curvature in these plots. Data for the two Nd:YAG lasers are plotted in Figs. 31 and 32. Deviations from linearity are evident at the high-power end of these plots (corresponding to the wings of the distribution),

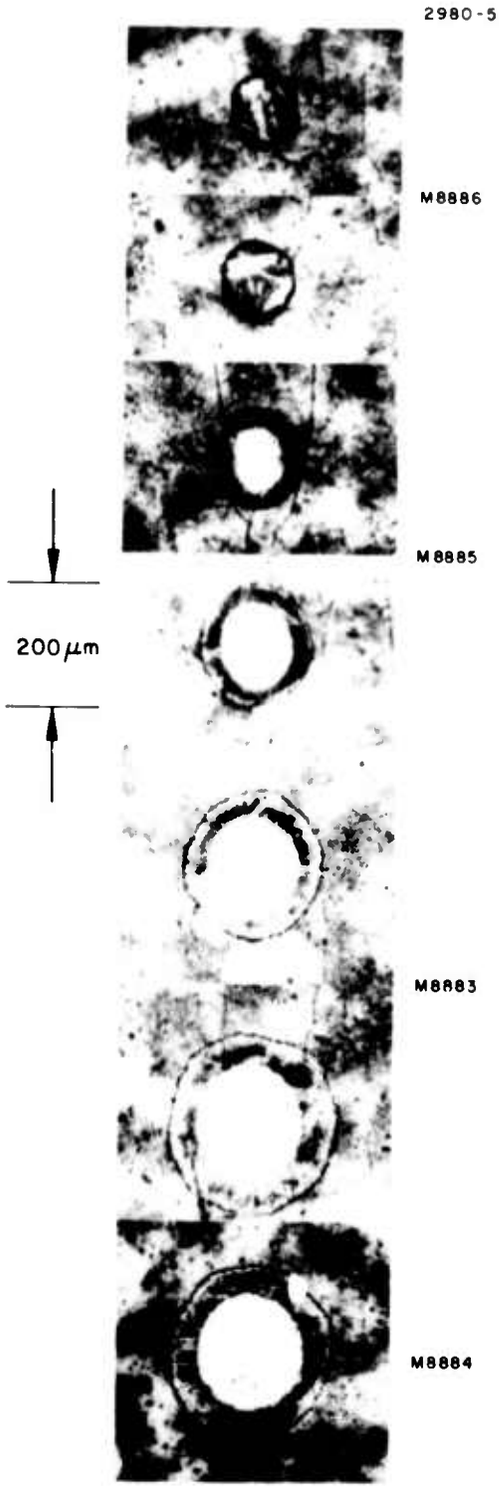

Fig. 30. Photomicro-raphs of Nd:YAG laser burn spots on polaroid film for different incident powers.

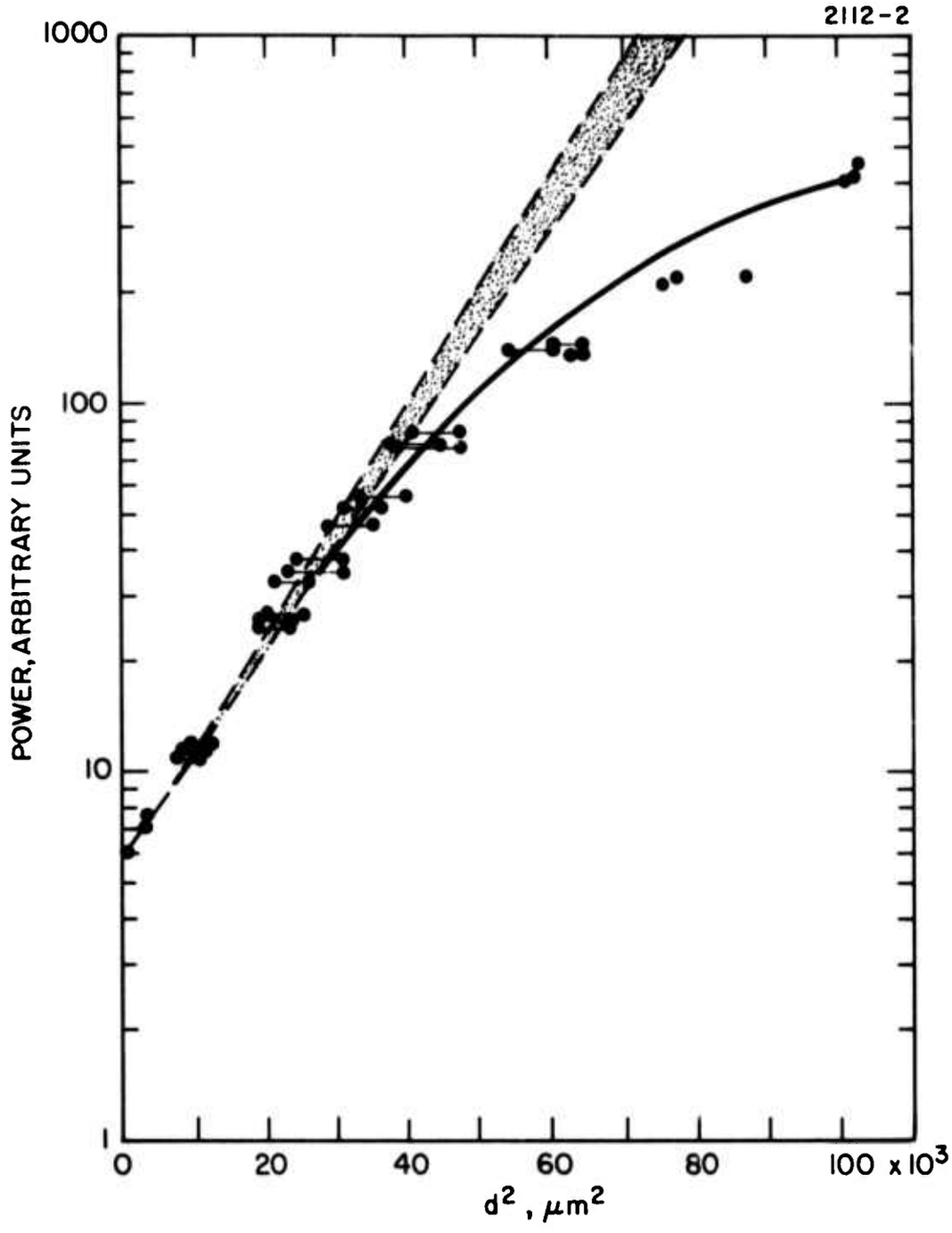

Fig. 31. Log P versus d^2 for burn spots taken at focus for high-power Nd:YAG laser.

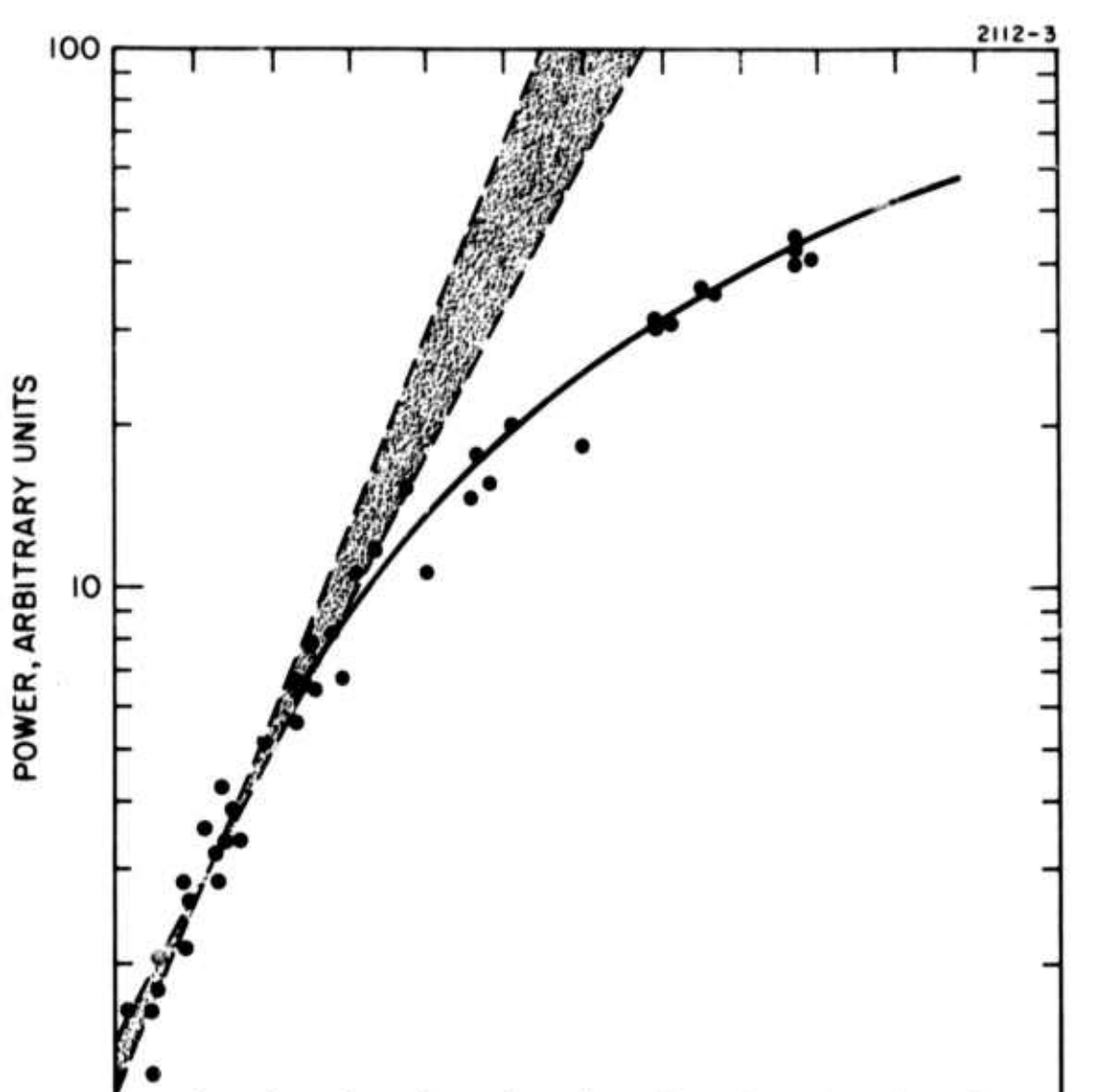

Fig. 32. Log P versus d^2 for burn spots taken at focus for low-power Nd:YAG laser.

and the curvature is such that the actual beam profile contains more energy in the wings than an ideal gaussian distribution. That is, the burn spots formed at high powers are larger than those expected for gaussian beams.

2. Beam Diagnostics at 6943 Å

A detailed series of beam profile and spot size measurements on the single-pulse ruby laser have been carried out in connection with another program.[6] The beam was photographed using a multiple exposure camera incorporating nine lenses, each one having a different amount of optical attenuation. Hence, each photograph contains nine different exposures of the same spot. By taking densitometer scans of the different spots, detailed information can be obtained about the spatial beam profile without requiring knowledge of the film response characteristics.[15] The results of a series of beam profile measurements are included in Ref. 6. The far-field spatial profile was found to be gaussian down to 8% of the peak. The spot size at the beam waist under the focusing conditions (19 cm lens) for the experiments carried out in this program for the pulsed ruby laser is 56 μm radius at the 1/e points for the electric field.

3. Power Calibration Measurements

For the pulsed ruby and high-power pulsed Nd:YAG lasers, the output energy was measured using a calibrated Hadron thermopile and simultaneously comparing the measured energy with the output of the monitoring Si photodetectors. From that point, the Si photodiodes were used as secondary standards. The energy of a single pulse was measured with the ruby laser while the total energy in a series of ten pulses was typically measured for the Nd:YAG laser operating at 10 pps. The energy per pulse was then obtained by dividing the total energy by the number of pulses. Temporal peak powers quoted in this report are obtained by dividing the total energy per pulse by the pulsewidth (FWHM). Power calibrations for the low-power Nd:YAG laser were carried out by measuring the average power in the

beam using a CRL Model 201 power meter, while the laser was operating at a given known pulse repetition rate and simultaneously monitoring the output of the photodetector monitor. Hence, from a knowledge of the repetition rate, average power, and pulsewidth, values of peak power and energy per pulse can be obtained.

III. THE NATURE OF OPTICAL BREAKDOWN IN CRYSTALS

A. Historical Background and Introduction

This project is but a small fraction of the considerable research and developmental effort currently being expended to develop windows, coatings, and other optical materials for high-power lasers. One objective of this and other efforts has been to understand and avoid high-field optical damage and breakdown. * As a result of this research, performed during the past few years, it is now known how to isolate and study bulk optical breakdown that does not arise from inclusions,[3,11] is not complicated by self-focusing of the damaging beam,[30-32] and can be calibrated because of effective beam mode control.[3,11,30-32]

1. A First Conclusion

One of the main conclusions that has been drawn from the careful experimental studies of optical breakdown is that the "intrinsic" breakdown field strengths have at last been observed and measured in ten alkali-halides,[30-32] sapphire,[33], quartz,[34] ZnSe,[34] and a few other transparent materials.[34] By "intrinsic" is meant that field strength that is characteristic of the ideal or pure material, and independent of whatever accidental impurities happened to exist in the materials.

2. A Second Conclusion

For reasons we summarize in Section III-C, it is widely stated that the mechanism for this breakdown has been established in these materials as being avalanche ionization of electrons across the insulating bandgap.[30-35] However, in the picosecond pulse regime it is thought that multiphoton absorption should dominate.

---

*We shall concern ourselves only with "high-field" damage here, even when it is not specifically stated. That is, we do not consider the damage that can occur via the heating produced by the small linear optical absorption that still persists even in the most transparent of optical materials.

3. A Third Conclusion

Experiments on surface damage threshold have indicated that the more perfectly prepared the surface, the closer is its damage threshold field to the bulk value.[36] It is, therefore, tentatively assumed that intrinsic surface breakdown has been observed and that its mechanism is avalanche ionization as it is thought to be for bulk damage.

4. Alternate Possibilities

In this project we have reviewed the evidence for the above conclusions, since they are so important for the direction of present and future research in optical damage. In Section III-B we will summarize the most pertinent experimental evidence bearing on these conclusions. In Sections III-C and III-D we review current theoretical interpretations of this evidence for dc and ac breakdown, respectively. Then, in Section III-E we show that the following alternate conclusions are also consistent with the data and existing, very crude, theoretical treatments of avalanche breakdown:

- The optical damage that has been observed to date, under conditions in which it was thought to be intrinsic, may have been, in every case, mediated by impurities, and therefore, not characteristic of pure or ideal materials.

- The mechanism of optical breakdown observed when inclusion damage, electron tunneling, and catastrophic self-focusing could be ruled out may not have arisen from avalanche ionization across the gap, but rather from the ionization of impurities (probably by an avalanche process) and the subsequent free-carrier absorption. This possibility was proposed early in this project, before the major experimental results we have mentioned had been accumulated.[9]

In the concluding Section III-F of this part of the report, we discuss the main items of practical importance that may be affected by one's choice of interpretation of the damage mechanism. These are primarily (1) the possible raising of damage threshold by the material

purification presently being attempted for other reasons, and (2) the possible existence of significant prebreakdown photoconductivity and its effect on optical propagation.

B. Experimental Evidence Bearing on Optical Breakdown Mechanisms

1. Similarity to DC Breakdown

The most striking feature of the rms optical threshold breakdown fields when they were first measured by Yablonovitch[30] at 10.6 μm in the alkali halides was their closeness, both in absolute and relative values, to the dc breakdown fields measured 35 years earlier by von Hippel in the same materials.[37] Furthermore, practically no change in these thresholds was seen by Fradin, et al., at 1.06 μm.[31] Perhaps a small increase (~25%) was seen in these thresholds when they were remeasured at 0.69 μm by Fradin and Bass.[32]

2. DC Breakdown Theories

There exists a vast literature attempting to analyze and understand dc breakdown thresholds.[38] In insulating materials, and at the temperatures of interest here, a theoretical concensus was developed after some years that the mechanism was avalanche ionization across the bandgap of the materials.[38] However, the theories on which this concensus was based were often mutually inconsistent and always approximate, since no success was achieved in solving for the actual electron energy distribution under realistic conditions. One of the most cogent theoretical discussions of the whole problem was that of Seitz[39] who sums up his findings with the remark (on his p. 1393): "The breakdown field ... estimated with the use of avalanche theory ... for NaCl is about 0.3×10^6 V/cm. The difference between this and the observed value of 1.5×10^6 V/cm ... indicates the approximate character of the equations." (Note: This discrepancy corresponds to a factor of 25 in optical breakdown intensity.)

3. AC Breakdown Theories

Existing ac (optical) breakdown theories, in which electrons in the conduction band of the crystal collide with phonons, are on even shakier ground than the dc theories.[9] However, theories of microwave avalanche ionization in gases, where the free electrons collide mainly with heavy neutral atoms, are more advanced. To a good approximation in these theories, the breakdown threshold field E_ω at frequency ω is related to E_o the dc breakdown field by

$$E_\omega = E_o(1 + \omega^2\tau^2)^{1/2} \quad (4)$$

where τ is a characteristic collision time. If this were also true in crystals, then the observed optical frequency dependence of E_ω in alkali halides is understandable. There is reason to expect $\omega\tau \sim 1$ at 1 μm. This fact establishes one link between gaseous avalanche ionization theory and observations in crystals.

4. Temperature Dependence

Buehl and von Hippel observed little change in E_o for KBr when the temperature was elevated from 0 to 200° C.[40] Kaseta and Li found little variation similarly in KCl.[41] When Yablonovitch saw little variation in E_ω for KCl in the same temperature range, he considered it a confirmation of (4).[30]

5. Dependence of Breakdown on Electric Field Direction and Polarization

Von Hippel early found no dependence of E_o on its direction with respect to alkali halide crystal axes.[37] Yablonovitch saw no change in E_ω as its direction of linear polarization was changed in alkali halides.[30] Giuliano (this report) saw no change in the breakdown intensity for sapphire at 6943 Å (1) as the direction of linear polarization was changed or (2) if circularly polarized light was used.

6. Impurity Dependence

Buehl and von Hippel saw a fairly smooth change in E_o as the concentration of K in mixed KCl-RbCl crystals was varied from 0 to 1.[40] Fradin, et al.,[34] found a similar smooth variation in E_ω at 1.06 μm for single crystal KBr-KCl alloys. These observations were taken to show that impurities caused little change in the threshold fields of the pure crystals.

7. Spark Spectra

Optical or dc damage in inclusion-free transparent insulators is invariably accompanied by a visible spark.[3, 11, 30-41] The only spectral resolution of such a spark known to us is that of Belikova, et al.,[42] who observed broad optical emission bands from sapphire near 2, 2.7, and 3 eV in a spectrometer whose range was 2 to 4 eV.

8. Recombination Radiation

Although recombination radiation has never been looked for from the breakdown spark, electrons in the conduction bands of alkali halides are known to recombine with holes mainly radiatively. That is why alkali halide crystals are used as scintillator crystals.

9. Impurity Levels in "Pure" Crystals

Recently R. Pastor has made an emission-spectrographic analysis of the impurity content of some standard Harshaw KCl crystals which were presumably very similar to the crystals used in optical breakdown experiments.[43] Metal-ion impurities, principally Mg and Ca, were found in concentrations of order 2×10^{19} per cc and other impurities such as Si, though not detected, could have been as numerous as 5×10^{19} per cc.

These crystals were grown from similar starting materials, and by similar techniques, as those used by von Hippel 35 years ago. Von Hippel obtained his samples from Professor Stockbarger who developed Harshaw's growth procedures. It would appear safe to

assume that these impurity levels were characteristic of all alkali halide crystals used over the years in breakdown measurements.

10. Defect Levels in "Pure Crystals

We have not yet sifted reports on the defect levels (interstitials, vacancies, etc.) in alkali-halide and other laser materials, but this will be pursued. Practically any defect imaginable could have an effect on breakdown.

C. Theoretical Interpretations of DC Breakdown

Of the half-dozen or so crude theories of avalanche ionization across the gap, some give remarkably good predictions of E_o in alkali halides at room temperature. Outstanding among these is the theory of Frohlich[44] about which Whitehead says in his book,[45] "... The agreement between theory and experiment is good, particularly when it is borne in mind that there are no disposable constants in the formula, a feature in which Frohlich's theory is unique and impressive."

However, Seitz criticizes this theory on several conceptual grounds.[39] Eventually, however, despite criticisms of all such theories, their general qualitative agreement with experimental thresholds, and the evidence of Sections III-B-4 and III-B-6, has led to the concensus that dc breakdown, once it had been made reproducible, was occurring because of avalanche ionization across the gap, and hence was characteristic of an ideal, pure material. Such impurities as existed were presumed to be playing no role in breakdown, partly because of evidence (Section III-B-6).

It was recognized that at high enough temperatures thermal runaway could cause breakdown, and for short enough pulses or thin enough samples. Zener tunneling could be responsible.[38] However, under normal conditions, avalanche ionization of valence electrons was presumed responsible. The only evidence that was difficult to understand on this hypothesis was that of Section III-B-5. Avalanching should be sensitive to the direction in the crystal in which it is occurring; the electron band structure is known to be very anisotropic at

high electron momenta[39]. Nevertheless, E_o appeared to be the same, in whatever direction it was applied.

D. Theoretical Interpretations of Optical Breakdown

Because there is good reason to believe that $\omega \lesssim 1$ at 10, 1, and 0.6 μm in the crystals in which optical breakdown has been studied, it has been argued on the basis of (4) that the theoretical interpretation of optical breakdown must be essentially the same as for dc breakdown (at room temperature, with no inclusions, etc.). Also, the numerical similarity of optical and dc breakdown thresholds has led to the hypothesis that the theory of ac breakdown must follow closely that for dc. That is, optical breakdown occurs by an ionizing avalanche of electrons across the crystal bandgap. We see, however, that alternate theories may be fruitful.

E. Proposed Alternate Interpretation

The evidence reviewed above suggests to us that both the dc and optical breakdown that have been studied may not be intrinsic but mediated by impurities. First, we point out some seeming inconsistencies in the "intrinsic" interpretation, and then discuss how impurity mechanisms would not present such difficulties, while being consistent with the other evidence which the intrinsic avalanche ionization hypothesis purports to explain.

1. Variation of Breakdown Strength with Frequency

Previous theories of how breakdown scales with frequency have concentrated on the relation of the electron scattering rates, possibly as a function of their energy, to the breakdown field oscillation frequency ω. However, there is a critical ω above which other physical considerations enter. This is the frequency ω_c at which fields of the observed breakdown intensity cannot possibly accelerate an electron to ionizing energies, in the absence of collisions. Above ω_c the maximum electron velocity remains below $(2U_i/m)^{1/2}$ where U_i is the energy needed to ionize and m is an effective electron mass.

If the velocity of an electron of effective mass m and charge e is exposed to an oscillating electric field $E_\omega \cos(\omega t + \phi)$ in the x direction, the maximum change in velocity that it can gain from the field, with no collisions, is

$$v_m = \frac{2e E_\omega}{m\omega} \tag{5}$$

which occurs after an appropriately timed half-cycle. The maximum energy produced by the field, in the absence of collisions, is

$$\frac{1}{2} m(v_o + v_m)^2 \tag{6}$$

where v_o is the initial velocity in the x direction. At the optical frequencies studied ($\geq 3 \times 10^{13}$ Hz) and typical breakdown fields $E_\omega \sim 10^6$ V/cm,

$$\frac{1}{2} m v_m^2 = \frac{2e^2 E_\omega^2}{m\omega^2} \tag{7}$$

is a very small fraction of a Rydberg (R) which is typical of the estimated electron energy for efficient lattice ionization. For example, at $\lambda = 10.6$ μm and a bare electron mass

$$\frac{1}{2} m v_m^2 \rightarrow 8.22 \times 10^{-3} [E_\omega (\text{MV/cm})]^2 \text{ R}. \tag{8}$$

The largest E_ω reported by Yablonovitch for 10.6 μm was 2.76 MV/cm for NaCl, whence the most energy a noncolliding electron with $v_o = 0$ could gain is 6.25×10^{-2} R, far too little to ionize. Other cases are worse.

The existence of an initial thermal velocity v_o would not increase the chances of achieving an ionizing energy in (6) appreciably. Therefore, even at the lowest optical frequencies studied, we have passed the characteristic frequency ω_c (never passed in microwave breakdown experiments!) where it is no longer possible to ionize the lattice with a noncolliding electron in the field.

For the above reasons, Bass[33] has proposed that an electron reaches ionizing energies by a series of "lucky" collisions, after each of which the electron in the conduction band has the right velocity to gain energy from the field before the next collision. In some sense this would certainly have to happen in a perfect crystal.

But if one depended on such lucky electrons to ionize the lattice, one would expect a steep rise in the threshold field E_ω as one went from 10.6 to 1.06 to 0.69 μm. It is easy to estimate that the minimum number N_ℓ of successive lucky collisions required in this process is

$$N_\ell \approx \sqrt{\frac{U_i}{2m}}\left(\frac{m\omega}{e\,E_\omega}\right) \tag{9}$$

where U_i is the energy needed to ionize. We see that the number of successive lucky collisions increases proportionally to ω. The probability P_ℓ that an electron will undergo such a lucky sequence must decrease faster than

$$P_\ell \leq (p_1)^{N_\ell} \tag{10}$$

where p_1 is the probability of the first collision being lucky at low electron energies.

A lucky collision must nearly reverse the momentum of the electron so that it can continue to gain energy after the optical field has reversed. A collision which reverses the momentum becomes less likely as the electron gains momentum and energy.

Therefore, we would expect the threshold field E_ω to increase proportionally to ω for $\lambda \leq 10.6$ μm, or

$$E_\omega \propto \omega \tag{11}$$

in order to keep the required number of lucky collisions N_ℓ from suffering an extremely improbable increase. This condition is the same as would be obtained from (4) for $\omega\tau >> 1$, but it arises from different physical considerations and seems to set in before $\omega\tau$ reaches 1.

That E_ω does not show this increase at $\lambda < 10.6$ μm suggests that ionization across the gap may not be the source of breakdown.

We note that if one needed only ionize impurities which required a fraction of an electron volt, the relative independence of E_ω on ω would be easier to understand in the above argument.

2. Polarization Independence of Thresholds

We pointed out in Section III-B-5 that the observed independence of breakdown at the direction of E relative to crystal axes at dc, or for linearly polarized ac radiation, was difficult to understand if conduction electrons had to achieve many electron volts of energy to participate in damage. Just as difficult to understand are further results in this report showing circularly polarized light to be just as damaging as linearly polarized light.

However, if electrons did not have to become so energetic to achieve damage, they would not move in the anisotropic parts of the conduction bands, and these observations would become understandable. We next demonstrate that such is likely if impurities mediate damage by creating free-carrier absorption.

3. Proposed Role of Known Impurities in Damage

Since Pastor has demonstrated that at least 10^{19} electrically active impurities exist per cubic centimeter in alkali halide crystals under study, let us suppose that the strong dc or ac fields first promote electrons from these impurities into the conduction

bands of the crystals before they perform the energetically more difficult task of promoting valence electrons. What would the free carrier absorption β cm^{-1} be? The common expression for β is

$$\beta = \frac{4\pi\rho e^2}{mnc\tau(\omega^2 + \tau^{-2})} \tag{12}$$

where ρ is the number density of electrons, n is the refractive index, and τ is an effective collision time which in damage studies is thought to be of order ω^{-1}. For free electron parameters, $\omega\tau = 1$, $\omega = 6\pi \times 10^{13}$ sec^{-1}, $n = 1.5$ and $\rho = 10^{19}$ cm^{-3},

$$\beta \rightarrow 2 \times 10^3 \text{ cm}^{-1} \tag{13}$$

from free-carrier absorption.

The energy per unit volume U_v(J cm^{-3}) deposited from a laser pulse of energy I J/cm^2 attenuated by β is

$$U_v = I\beta \ . \tag{14}$$

For the 10 J/cm^2 pulse that are typically seen to initiate damage,

$$U_v \sim 2 \times 10^4 \text{ J/cm}^3 \tag{15}$$

for the ionized impurity parameters considered above. Such energy depositions are clearly above the range that would be expected to cause damage. Therefore, if only a small fraction ($\lesssim 1/10$) of the metal ion impurities known to be present in "pure" alkali halide crystals were ionized, free carrier absorption of laser pulses known to cause damage would be well into the catastrophic regime. This mechanism would never require the electrons to become very energetic, as we see in the next section.

4. Ionization of Impurities

The ionization of impurities can proceed by ordinary one-photon absorption. However, it is unlikely that a significant fraction are ionized by this process. If the recombination time of ionized impurities τ_r were less than the laser pulse duration τ_p, then during the pulse there would be an equilibrium density ρ_o from single photon excitation:

$$\rho_o \sim \beta_o \tau_r I/(\hbar\omega \tau_p) , \tag{16}$$

where β_o is the contribution to the crystal absorption coefficient from these impurities and τ_p is the pulse duration. From experiments on alkali halides $\beta_o < 10^{-4}$ cm^{-1} and $\tau_r \lesssim 10^{-1} \tau_p$. For the several Joule cm^{-2} levels seen to damage, $I \sim 10^{20}$ $\hbar\omega$ at 10.6 μm. Therefore, ρ_o is not expected to be above 10^{15} cm^{-3} from single-photon excitation, a value which is unlikely to produce damage. We cannot entirely rule this process out, however, should τ_r prove to be longer than estimated above. Furthermore, we can say that multiphoton absorption is even less likely than single-photon absorption at GW per cm^2 levels.

The ionization of impurities also can be produced by an avalanche process. The presence of a conduction electron is known to enhance the probability of the light beam exciting a nearby impurity electron.[9] The conduction electron absorbs or contributes energy and momentum needed for the excitation. This is, of course, the basic step in a potential avalanche process. Without knowing the nature and energy of the ~10^{19} cm^{-3} bound impurities typical in alkali-halides, it is difficult to make quantitative estimates of avalanche rates. But it was shown in Ref. 9 that a simple and reasonable impurity potential gives avalanche cross sections that would lead to breakdown at typical intensities.

5. Conclusions of this Study

In the optical regimes where breakdown is studied, a conduction electron must undergo a sequence of lucky collisions to reach ionizing energies. To keep the rather low probability of this "lucky" sequence from dropping as the optical frequency ω is increased, the electric field strength must increase proportionally with ω. Therefore, one would expect optical damage threshold intensities to be ~100 times higher at 1 μm wavelengths than at 10 μm. In fact, they are the same to within 10%.[31] Surely, this lucky electron picture is not so wrong as to mislead by such a factor. Therefore:

- The model of electrons being ionized across the crystal bandgap in avalanche is at odds with the experimentally observed wavelength independence of breakdown thresholds.
- The observed independence of breakdown threshold on field polarization is difficult to understand if hot electrons are causing impact ionization across the gap.
- The observed high density of metal ion impurities ($\sim 10^{19}$ cm^{-3}) in the alkali halides under study should affect damage thresholds. For example, 10^{18} conduction electrons per cubic centimeter would cause catastrophic heat deposition by free-carrier absorption. It is difficult to imagine how these impurity electrons could be passed by in any electron avalanche process.

F. Summary and Recommendations

We believe our studies have established doubt as to the correctness of the standard interpretation of the most careful recent optical breakdown studies. This interpretation holds that "intrinsic" breakdown strengths, independent of impurities, have been measured. Rather, it seems possible that ionic impurities, now known to exist in the best crystals studied to date, play a crucial role in optical breakdown.

1. Suggested Further Studies

The opposing interpretations given above differ drastically in their predictions of the energies of empty electronic states (holes) just before and during optical breakdown. Conventional theories would have many holes in the crystal valence band, whereas ours would not. Therefore, a study of the spectrum of the electron-hole recombination radiation should be able to decide from which states the conduction electrons (which all agree are being created) are excited.

Prebreakdown measurements of photoconductivity versus exciting wavelength would yield a picture of the impurity level structure and density. From these, projections could be made of avalanche thresholds.

The density of imperfections other than foreign ions should be studied, and its effect on the rate of "lucky" collisions, electron traps, etc.

2. Practical Implications of Mechanisms

It is not clear how low impurity densities would have to be achieved in order to effect an appreciable change in optical breakdown thresholds; perhaps too low to be easily achieved. However, neutralization of the ability of existing impurities to supply electrons and the deep trapping of electrons produced could increase damage thresholds.

REFERENCES

1. C. R. Giuliano, "Laser-Induced Damage to Transparent Dielectric Materials," Appl. Phys. Letters 5, 137-139 (1964).

2. Damage in Laser Glass, American Society for Testing and Materials Technical Publication No. 469, edited by A. Glass, A. Guenther, C. Stickely, and J. Myers (American Society for Testing and Materials, Philadelphia, Pa., 1969).

3. Damage in Laser Materials, edited by A. J. Glass and A. H. Guenther, U. S. National Bureau of Standards Special Publication No. 341 (U. S. GPO, Washington, D. C., 1970).

4. Damage in Laser Materials, edited by A. J. Glass and A. H. Guenther, U. S. National Bureau of Standards Special Publication No. 356 (U. S. GPO, Washington, D. C., 1971).

5. Laser Induced Damage in Optical Materials: 1972, edited by A. J. Glass and A. H. Guenther, U. S. National Bureau of Standards Special Publication No. 372 (U. S. GPO, Washington, D. C., 1972).

6. C. R. Giuliano, D. F. DuBois, R. W. Hellwarth, L. D. Hess, and G. R. Rickel, "Damage Threshold Studies in Laser Crystals," Final Technical Report, Contract F19628-69-C-0277, ARPA Order No. 1434, September 1972.

7. C. R. Giuliano and D. Y. Tseng, "Laser Induced Damage to Nonlinear Optical Materials," Final Report, Contract F33615-71-C-1715, September 1972.

8. C. R. Giuliano and L. D. Hess, "Damage Threshold Studies in Ruby and Sapphire," National Bureau of Standards Special Publication 341, U. S. GPO, Washington, D. C., December 1970, p. 76 (ed. by A. J. Glass and A. H. Guenther).

9. R. W. Hellwarth, "Role of Photo-Electrons in Optical Damage," National Bureau of Standards Special Publication 341, U. S. GPO, Washington, D. C., December 1970, p. 67 (ed. by A. J. Glass and A. H. Guenther).

10. C. R. Giuliano, "Time Evolution of Damage Tracks in Sapphire and Ruby," National Bureau of Standards Special Publication 356, U. S. GPO, Washington, D. C., November 1971, p. 44 (ed. by A. J. Glass and A. H. Guenther.

11. C. R. Giuliano and J. H. Marburger, "Observations of Moving Self-Foci in Sapphire," Phys. Rev. Letters 27, 905 (1971).

12. C. R. Giuliano, "Laser-Induced Damage in Transparent Dielectrics: Ion Beam Polishing as a Means of Increasing Surface Damage Thresholds," Appl. Phys. Letters 21, 39 (1972).

13. C. R. Giuliano, J. H. Marburger, and A. Yariv, "Enhancement of Self-Focusing Threshold in Sapphire with Elliptical Beams," Appl. Phys. Letters 21, 58 (1972).

14. C. R. Giuliano, "Laser-Induced Damage in Transparent Dielectrics: The Relationship between Surface Damage and Surface Plasmas," IEEE-J. Quantum Electronics 8, 749 (1972).

15. R. W. Hellwarth, "Fundamental Absorption Mechanisms in High Power Laser Window Materials," National Bureau of Standards Special Publication 372 (U.S. GPO, Washington, D. C., 1972) p. 165 (edited by A. J. Glass and A. H. Guenther).

16. C. R. Giuliano, "The Relation Between Surface Damage and Surface Plasma Formation," (Same as Ref. 15, p. 46).

17. C. R. Giuliano, "Ion Beam Polishing as a Means of Increasing Surface Damage Thresholds in Sapphire," (Same as Ref. 15, p. 55).

18. E. O. Ammann and J. M. Yarborough, Appl. Phys. Lett. 17, 233 (1970).

19. D. C. Hanna, B. Luther-Davies, H. N. Rutt, and R. C. Smith, Appl. Phys. Lett. 20, 34 (1972).

20. D. C. Hanna, B. Luther-Davies, and R. C. Smith, Appl. Phys. Lett 22, 440 (1973).

21. J. Warner, Appl. Phys. Lett. 12, 222 (1968).

22. Y. Klinger and F. Arams, Proc. IEEE 57, 1797 (1969).

23. D. Y. Tseng, Appl. Phys. Lett. 21, 382 (1972).

24. D. C. Hanna, B. Luther-Davies, H. N. Rutt, R. C. Smith and C. R. Stanley, IEEE-JQE 8, 317 (1972).

25. J. F. Ready, Effects of High-Power Laser Radiation (Academic Press, N.Y., 1971, Ch. 3.

26. E. S. Bliss, Damage in Laser Materials, edited by A. J. Glass and A. H. Guenther, U. S. National Bureau of Standards Special Publication No. 341. (U. S. GPO, Washington, D. C. 1970), p. 105.

27. R. C. Smith, University of Southampton, private communication.

28. N. Bloembergen, Applied Optics 12, 661 (1973).

29. I. M. Winer, "A Self-Calibrating Technique Measuring Laser Beam Intensity Distributions," Appl. Optics 5, 1437 (1966).

30. E. Yablonovitch, Appl. Phys. Lett. 19, 495 (1971).

31. D. W. Fradin, E. Yablonovitch, and M. Bass, Appl. Optics 12, 700 (1973).

32. D. W. Fradin and M. Bass, Appl. Phys. Lett. 22, 206 (1973).

33. D. Fradin, M. Bass, and L. Holoway, Jr., Raytheon Co., Final Report, Contract F19628-70-C-0223, February 1973.

34. D. W. Fradin, M. Bass, D. P. Bua, and C. A. Christian, Proceedings of the Third Conference on High-Power Laser-Window Materials, Hyannis, Massachusetts, November 1973.

35. N. Bloembergen, "Laser-Induced Electric Breakdown in Solids," a review (to be published in the IEEE Journal of Quantum Electronics).

36. D. W. Fradin and M. Bass, Appl. Phys. Lett. 22, 157 (1973).

37. R. W. Hellwarth, "Role of Photo-Electrons in Optical Damage," National Bureau of Standards Special Publication 341 (U. S. GPO, Washington, D. C., December 1970), ed. by A. J. Glass and A. H. Guenther.

38. A. von Hippel, J. Appl. Phys. 8, 815 (1937).

39. See, for example, J. J. O'Dwyer, The Theory of Dielectric Breakdown in Solids (Oxford University Press, 1964).

40. F. Seitz, Phys. Rev. 76, 1376 (1949).

41. R. C. Buehl and A. von Hippel, Phys. Rev. 56, 941 (1939).

42. F. W. Kaseta and H. T. Li, J. Appl. Phys. 37, 2744 (1966).

43. T. P. Belikova, A. N. Savchenko, and E. A. Sviridenkov, Sov. Phys.-JETP 27, 19 (1968).

44. R. C. Pastor and M. Braunstein, Hughes Research Laboratories Technical Report AFWL-TR-152, Vol. II (April 1973).

45. H. Frohlich, Proc. Roy. Soc. 160, 230 (1937); 172, 94 (1939); 178, 493 (1941); 188, 521, 532 (1947); Phys. Rev. 61, 200 (1942).

46. S. Whitehead, Dielectric Breakdown in Solids (Oxford, Clarendon Press, 1953).